Next-to-minimal supersymmetric model solution to the fine-tuning problem, precision electroweak constraints, and the largest CERN LEP Higgs event excess

Radovan Dermíšek[1] and John F. Gunion[2]

[1]*School of Natural Sciences, Institute for Advanced Study, Princeton, New Jersey 08540, USA*
[2]*Department of Physics, University of California at Davis, Davis, California 95616, USA*
(Received 14 June 2007; published 14 November 2007)

We present an extended study of how the next-to-minimal supersymmetric model easily avoids fine-tuning in electroweak symmetry breaking for a SM-like light Higgs with mass in the vicinity of 100 GeV, as beautifully consistent with precision electroweak data, while escaping LEP constraints due to the dominance of $h \to aa$ decays with $m_a < 2m_b$ so that $a \to \tau^+\tau^-$ or jets. The residual $\sim$10% branching ratio for $h \to b\bar{b}$ explains perfectly the well-known LEP excess at $m_h \sim 100$ GeV. Details of model parameter correlations and requirements are discussed as a function $\tan\beta$. Comparisons of fine-tuning in the NMSSM to that in the MSSM are presented. We also discuss fine-tuning associated with scenarios in which the a is essentially pure singlet, has mass $m_a > 30$ GeV, and decays primarily to $\gamma\gamma$ leading to an $h \to aa \to 4\gamma$ Higgs signal.

DOI: 10.1103/PhysRevD.76.095006 PACS numbers: 14.80.Cp, 12.60.Fr, 12.60.Jv

I. INTRODUCTION

In the standard model (SM), electroweak symmetry breaking, whereby the W and Z bosons and the quarks and leptons acquire mass, gives rise to a Higgs boson, $h_{\rm SM}$. However, the value of $m_{h_{\rm SM}}$ is quadratically sensitive to the cutoff scale of the theory, Λ, especially through top quark loops which give a one-loop correction of

$$\delta m^2_{h_{\rm SM}} = -\frac{3}{4\pi^2}\frac{m_t^2}{v^2}\Lambda^2, \tag{1}$$

where Λ is the high energy cutoff and $v = 176$ GeV. For Λ of order the GUT scale, M_U, or the Planck scale, $M_{\rm P}$, an extreme cancellation between the one-loop contribution(s) and the bare Higgs mass is required in order that the physical Higgs mass be below a TeV, as required in order for the scattering of longitudinally polarized W bosons to obey unitarity in a perturbative fashion.

Supersymmetric (SUSY) models, such as the minimal supersymmetric model (MSSM), cure this naturalness/hierarchy problem associated with the quadratically divergent 1-loop corrections via the introduction of superpartners for each SM particle. Because the spin of the superpartners differs by 1/2 unit from that of the corresponding SM particle, the 1-loop correction from the superpartner will cancel that of the SM particle once the energy scale being integrated over in the loop is above the mass of the (presumed to be heavier) superpartner. So long as the superpartners have mass somewhat below 1 TeV (say $\sim$500 GeV), the cancellation is not particularly extreme and the hierarchy/naturalness problem associated with the quadratic divergences is ameliorated. However, there remains the question of how finely the GUT-scale parameters must be adjusted in order to get appropriate electroweak symmetry breaking, that is to say correctly predict the observed value of m_Z. It is here that LEP limits on a SM-like Higgs boson play a crucial role.

Supersymmetric models most naturally predict that the lightest Higgs boson, generically h, is SM-like and that it has a mass closely correlated to m_Z, typically lying in the range $\lesssim 105$ GeV for stop masses $\lesssim 500$ GeV, with an upper bound, for example, of $\lesssim 135$ GeV in the MSSM for stop masses $\sim$1 TeV and large stop mixing. If the stop masses are large, the predicted value of m_Z is very sensitive to the GUT scale parameters. Such sensitivity is termed ''fine-tuning.'' Models with minimal fine-tuning provide a much more natural explanation of the Z mass than those with a high level of fine-tuning. The degree of fine-tuning required is thus quite closely related to the constraints on a SM-like h, and these in turn depend on how it decays.

The SM and the MSSM predict that $h \to b\bar{b}$ decays are dominant and LEP has placed strong constraints on $Zh \to Zb\bar{b}$. The limits on

$$C^{2b}_{\rm eff} \equiv [g^2_{ZZh}/g^2_{ZZh_{\rm SM}}]B(h \to b\bar{b}) \tag{2}$$

are shown in Fig. 1 (from Ref. [1]). From this plot, one concludes that $m_h < 114$ GeV is excluded for a SM-like h that decays primarily to $b\bar{b}$. In fact, because of the manner in which the analysis is done, at a first level of approximation this limit applies for an h that decays to any combination of $2b$ and $4b$. For $B(h \to b\bar{b}) \sim 0.15$ and $B(h \to b\bar{b}b\bar{b}) \sim 0.8$ (with τ channels making up the rest) $m_h \lesssim 110$ GeV is excluded. This will be important later. In the case of the CP-conserving MSSM, one always obtains $B(h \to b\bar{b}) \gtrsim 0.88$. For $m_{\rm SUSY} \lesssim 1$ TeV, most of parameter space will yield $m_h < 114$ GeV and thus be ruled out by the SM-like Higgs LEP limit. The remaining part of MSSM parameter space either has at least one very large parameter, most typically a soft-SUSY-breaking stop mass close to a TeV at scale m_Z, or else large mixing in the stop sector. In the former case, one always finds that to predict the observed m_Z requires very careful adjustment, i.e. fine-tuning, of the GUT-scale parameters with accuracies better

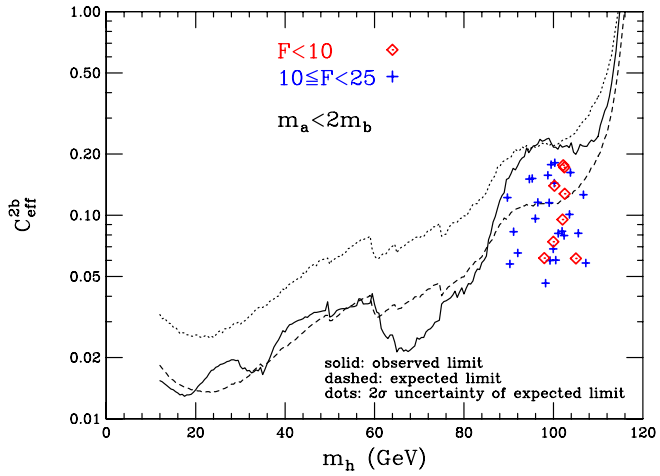

FIG. 1 (color online). Expected and observed 95% CL limits on $C^{2b}_{\rm eff}$ from Ref. [1] are shown vs. m_h. Also plotted are the predictions for the NMSSM parameter cases discussed in [3] having fixed $\tan\beta = 10$, $M_{1,2,3}(m_Z) = 100$, 200, 300 GeV that give fine-tuning measure $F < 25$ and $m_{a_1} < 2m_b$ and that are consistent with Higgs constraints obtained using the preliminary LHWG analysis code [4].

than 1%. In the latter case, fine-tuning can be reduced to the 3% level. To achieve small fine-tuning, let us say no worse than 10%, the soft-SUSY-breaking parameters that affect the Higgs sector should be well below a TeV, in which case the lightest CP-even MSSM Higgs boson would have mass $\sim$100 GeV.

As suggested in [2], the simplest way to allow a Higgs mass of order 100 GeV, thus making possible a light SUSY spectrum and low fine-tuning, is to modify Higgs decays so that the $b\bar{b}$ branching ratio is small and primary decays are to channel(s) to which LEP is less sensitive. This is very natural in models in which the Higgs sector is extended and Higgs to Higgs decays are kinematically allowed. The decay widths for Higgs to Higgs decays can easily exceed the very small width for the $b\bar{b}$ channel. The simplest supersymmetric model that gives rise to this possibility is the next-to-minimal supersymmetric model (NMSSM). The NMSSM yields a preferred value of $m_h \sim 100$ GeV purely on the basis of minimizing fine-tuning. A Higgs mass near 100 GeV is also strongly preferred by precision electroweak measurements. Further, there is a well-known 2.3σ excess in the $e^+e^- \to Z + b's$ channel in the LEP data for $M_{b's} \sim 100$ GeV when a final state that contains two or more $b's$ is assumed to contain exactly 2 $b's$. If the Higgs decays only to $b\bar{b}$ then this excess and limits on the $Z + b's$ final state would apply to $C^{2b}_{\rm eff}$ defined by

$$C^{2b}_{\rm eff} = [g^2_{ZZh}/g^2_{ZZh_{\rm SM}}]B(h \to b\bar{b}). \quad (3)$$

The excess is apparent in the higher observed vs expected $C^{2b}_{\rm eff}$ limits for a test Higgs mass of $m_h \sim 100$ GeV shown in Fig. 1. This excess is particularly apparent in the $1-CL_b$ result (Fig. 7 of [1]) obtained after combining all four LEP experiments.

In a previous paper [3], we have shown that the above excess is consistent with a scenario in which the Higgs boson has SM-like ZZh coupling, but has reduced $B(h \to b\bar{b})$ by virtue of the presence of h decays to a pair of lighter Higgs bosons, $h \to aa$, where $B(a \to b\bar{b})$ is small, as is automatic if $m_a < 2m_b$ so that $a \to \tau^+\tau^-$ or light quarks and gluons.[1] (The importance of such decays was first emphasized in [5], and later in [6], followed by extensive work in [7–10].) For example, if the ZZh coupling is full SM strength, then $m_h \sim 100$ GeV with $B(h \to b\bar{b}) \sim 0.08$ and $B(h \to aa) \sim 0.9$ fits the observed $Z2b$ excess nicely. Meanwhile, there are no current limits on the $Zh \to Zaa \to Z\tau^+\tau^-\tau^+\tau^-$ final state for $m_h \gtrsim 87$ GeV [11]. And limits in the case of $a \to$ jets run out at slightly lower m_h. As already stressed and as described below in more detail, we are particularly led to the above interpretation of LEP data since fine-tuning within the NMSSM is absent for model parameters that yield precisely this kind of scenario [2,3]. While various alternative interpretations of this excess in terms of a non-SM Higgs sector have been suggested [11,12], the NMSSM scenario has the lowest fine-tuning of any such scenario and has particularly strong theoretical motivation.

The NMSSM is an extremely attractive model [13]. First, it provides a very elegant solution to the μ problem of the MSSM via the introduction of a singlet superfield $\hat{S}$. For the simplest possible scale invariant form of the superpotential, the scalar component of $\hat{S}$ naturally acquires a vacuum expectation value of the order of the SUSY-breaking scale, giving rise to a value of μ of order the electroweak scale. The NMSSM is the simplest supersymmetric extension of the standard model in which the electroweak scale originates from the SUSY-breaking scale only. Hence, the NMSSM deserves very serious consideration.

Apart from the usual quark and lepton Yukawa couplings, the scale invariant superpotential of the NMSSM is $W = \lambda\hat{S}\hat{H}_u\hat{H}_d + \frac{1}{3}\kappa\hat{S}^3$ depending on two dimensionless couplings λ, κ beyond the MSSM. [Hatted (unhatted) capital letters denote superfields (scalar superfield components).] The associated trilinear soft terms are $\lambda A_\lambda S H_u H_d + \frac{1}{3}\kappa A_\kappa S^3$. The final two input parameters are $\tan\beta = h_u/h_d$ and $\mu_{\rm eff} = \lambda s$, where $h_u \equiv \langle H_u\rangle$, $h_d \equiv \langle H_d\rangle$ and $s \equiv \langle S\rangle$. The Higgs sector of the NMSSM is thus described by the six parameters λ, κ, A_λ, A_κ, $\tan\beta$, $\mu_{\rm eff}$. In addition, values must be input for the gaugino masses and for the soft terms related to the (third generation) squarks and sleptons that contribute to the radiative corrections in the Higgs sector and to the Higgs decay widths.

[1] If $a \to b\bar{b}$ is dominant, as occurs for $m_a > 2m_b$, then, as noted earlier in the text, $m_h \gtrsim 110$ GeV is required by LEP data [4].

The particle content of the NMSSM differs from the MSSM by the addition of one CP-even and one CP-odd state in the neutral Higgs sector (assuming CP conservation), and one additional neutralino. The result is three CP-even Higgs bosons ($h_{1,2,3}$) two CP-odd Higgs bosons ($a_{1,2}$) and a total of five neutralinos $\tilde{\chi}^0_{1,2,3,4,5}$. It will be convenient to denote the CP-even and CP-odd neutral Higgs bosons of the MSSM as h, H and A, respectively, while those of the NMSSM will be denoted by h_1, h_2, h_2 and a_1, a_2, respectively. In the latter case, our focus will be on the lightest states h_1 and a_1. The NMHDECAY program [14], which includes most LEP constraints, allows easy exploration of Higgs phenomenology in the NMSSM.

In [2,3], we presented a first study of the fine-tuning issues for the NMSSM vs the MSSM. We define the fine-tuning measure to be

$$F = \max_p F_p \equiv \max_p \left| \frac{d \log m_Z}{d \log p} \right|, \tag{4}$$

where the parameters p comprise all GUT-scale soft-SUSY-breaking parameters.

II. COMPARISON OF THE MSSM WITH THE NMSSM

In this section, we will consider scenarios associated with minimal fine-tuning in the MSSM and the NMSSM. In the following section, we will give a broader overview of all types of NMSSM scenarios and will show how it is that one is lead to the NMSSM scenarios considered in this section.

We discuss fine-tuning for the MSSM first. In this case, the GUT-scale parameters comprise: $M_{1,2,3}$, μ, B_μ, m_Q^2, m_U^2, m_D^2, m_L^2, m_E^2, $m_{H_u}^2$, $m_{H_d}^2$, A_t, A_b, and A_τ. In principle, soft masses squared for the first two generations should be included above, but they have negligible effect upon m_Z. In our approach, we choose m_Z-scale values for all the squark and slepton soft masses squared at scale m_Z, for the gaugino masses, $M_{1,2,3}(m_Z)$, and for $A_t(m_Z)$, $A_b(m_Z)$ and $A_\tau(m_Z)$ (with no requirement of universality at the GUT scale). We also choose m_Z-scale values for $\tan\beta$, μ and m_A; these uniquely determine $B_\mu(m_Z)$. The vevs h_u and h_d at scale m_Z are fixed by $\tan\beta$ and m_Z via $m_Z^2 = \bar{g}^2(h_u^2 + h_d^2)$ (where $\bar{g}^2 = g^2 + g'^2$). Finally, $m_{H_u}^2(m_Z)$ and $m_{H_d}^2(m_Z)$ are determined from the two potential minimization conditions. [From here on, all parameters displayed without an explicit argument are m_Z-scale values, although we sometimes give them an explicit (m_Z) argument for emphasis. All GUT-scale parameters will be specifically indicated using an explicit argument (M_U).] We then evolve all parameters to the MSSM GUT scale (including μ and B_μ). Next, we shift each of the GUT-scale parameters in turn, evolve back down to scale m_Z, and reminimize the Higgs potential using the shifted values of μ, B_μ, $m_{H_u}^2$ and $m_{H_d}^2$. This gives new values for h_u and h_d from which we compute a new value for m_Z (and $\tan\beta$).

It is not difficult to understand why fine-tuning is typically large in the MSSM given LEP constraints. Minimization of the Higgs potential gives (at scale m_Z)

$$\frac{1}{2} m_Z^2 = -\mu^2 + \frac{m_{H_d}^2 - \tan^2\beta m_{H_u}^2}{\tan^2\beta - 1}. \tag{5}$$

The m_Z-scale μ, $m_{H_u}^2$, $m_{H_d}^2$ parameters can be determined from the GUT-scale values of all SUSY-breaking parameters via the renormalization group equations (RGEs). The result for $\tan\beta = 10$ (similar to the $\tan\beta = 2.5$ results in Refs. [15,16]) is

$$\begin{aligned} m_Z^2 \sim & -2.0\mu^2(M_U) + 5.9M_3^2(M_U) + 0.8m_Q^2(M_U) \\ & + 0.6m_U^2(M_U) - 1.2m_{H_u}^2(M_U) - 0.7M_3(M_U)A_t(M_U) \\ & + 0.2A_t^2(M_U) + \ldots \end{aligned} \tag{6}$$

All of the above terms aside from $-2\mu^2(M_U)$ and $-2m_{H_u}^2(M_U)$ arise from the RGE evolution result for $2m_{H_u}^2(M_U) - 2m_{H_u}^2(m_Z^2)$. Similarly, one can expand m_Z-scale values for soft-SUSY-breaking parameters in terms of GUT-scale parameters. In particular, one finds (at $\tan\beta = 10$)

$$A_t(m_Z) \sim -2.3M_3(M_U) + 0.24A_t(M_U) \tag{7}$$

$$M_3(m_Z) \sim 3M_3(M_U) \tag{8}$$

$$\begin{aligned} \bar{m}_{\tilde{t}}^2(m_Z) \sim & \; 5.0M_3^2(M_U) + 0.6\bar{m}_{\tilde{t}}^2(M_U) \\ & + 0.2A_t(M_U)M_3(M_U). \end{aligned} \tag{9}$$

In the above,

$$\bar{m}_{\tilde{t}} \equiv [\tfrac{1}{2}(\bar{m}_{\tilde{t}_1}^2 + \bar{m}_{\tilde{t}_2}^2)]^{1/2}. \tag{10}$$

Unless there are large cancellations (fine-tuning), one would expect that

$$m_Z \sim m_{\tilde{g}}, \bar{m}_{\tilde{t}}, m_{\tilde{H}^\pm}, \tag{11}$$

where $m_{\tilde{H}^\pm}$ is similar in size to μ. We would need a very light gluino, and a rather light stop, to avoid fine-tuning. More precisely, if $A_t(M_U) = 0$, then it is clear from Eq. (6) that the minimum of F is determined by the $5.9M_3^2(M_U)$ term, which would give $F \sim 6$ for $M_3(M_U) = 300$ GeV. Allowing for small positive $A_t(M_U)$ reduces this minimum F somewhat, as will be illustrated below. Of course, in specific models you can also have correlations among the GUT-scale parameters that would reduce F.

The problem is that the small A_t value required for minimal F does not yield a MSSM Higgs mass m_h above the 114 GeV LEP limit unless $\bar{m}_{\tilde{t}}$ is very large (which causes a high level of fine-tuning, $F > 175$). To maximize m_h at moderate $\bar{m}_{\tilde{t}}$, one should consider parameters corresponding to $|A_t/\bar{m}_{\tilde{t}}| \sim \sqrt{6}$, termed an "$m_h$-max scenario."

For such choices it is also possible to obtain $m_h > 114$ GeV. To simultaneously minimize F, the sign of A_t must be chosen negative. To understand this, we first note that $m_h > 114$ GeV can be achieved with $-A_t \gtrsim 500$ GeV or $A_t \gtrsim 500$ GeV and $\bar{m}_{\tilde{t}} \sim 300$ GeV. Given Eq. (9), this translates to $-A_t(M_U) \gtrsim 1$ TeV or $A_t(M_U) \gtrsim 3$ TeV, respectively. In both cases, F will be determined by the $0.2A_t^2(M_U)$ term in Eq. (9), yielding

$$F \sim 0.2\frac{A_t^2(M_U)}{m_Z^2}. \tag{12}$$

Obviously the case of $A_t(M_U) \gtrsim 3$ TeV case will correspond to very large fine-tuning, roughly $F \gtrsim 180$. For the $-A_t(M_U) \gtrsim 1$ TeV case, $F \gtrsim 30$ is obtained. Similar values of F can be obtained for much smaller $|A_t(M_U)|$ values provided one allows for moderate $\bar{m}_{\tilde{t}}^2(M_U) < 0$ [17].

The above generic features are apparent in the numerical results presented in Fig. 2 for the case of $\tan\beta(m_Z) = 10$ and $M_{1,2,3}(m_Z) = 100$, 200, 300 GeV. We scan randomly over $A_t(m_Z)$, $A_b(m_Z)$, $A_\tau(m_Z)$ and 3rd generation squark and slepton soft masses-squared above $(200\ \text{GeV})^2$, as well as over $|\mu(m_Z)| \geq 100$ GeV, sign$(\mu) = \pm$ and over $m_A > 120$ GeV. For such values of m_A, the h is quite SM-like and only allowed by LEP data if $m_h \gtrsim 114$ GeV. If lower values of m_A are allowed, in particular $m_A \sim 100$ GeV, lower values of $F \sim 16$ can be obtained for experimentally allowed scenarios. In these latter scenarios, the H is typically fairly SM-like but will have mass above 114 GeV while the h can have mass below 114 GeV by virtue having weak ZZ coupling. These scenarios are characterized by mixing among the Higgs bosons. Analogous mixed-Higgs scenarios are also possible in the NMSSM. The MSSM and NMSSM mixed-Higgs scenarios will be considered in a separate paper [18]. The fine-tuning in NMSSM mixed-Higgs scenarios have also been discussed in [19]. The main drawback of mixed-Higgs scenarios is that they require adjustments in other parameters besides those necessary for correct electroweak symmetry breaking.

Returning to Fig. 2, the top plot gives F as a function of $\bar{m}_{\tilde{t}}$. The latter enters into the computation of the radiative correction to the SM-like light Higgs mass m_h. In the middle plot, we display F as a function of m_h. And, in the bottom plot we display F as a function of A_t. We first of all note that the very smallest values of F are achieved for $\bar{m}_{\tilde{t}} \in [300\ \text{GeV}, 400\ \text{GeV}]$, $m_h \sim 90$–105 GeV and $A_t \in [-400\ \text{GeV}, 0]$. As stated above, for $m_A > 120$ GeV, as considered here, the h is fairly SM-like in all its couplings to SM particles. Thus, points with $m_h < 114$ GeV, plotted as (blue) +'s, are excluded by LEP data, whereas those with $m_h > 114$ GeV, plotted as (red) ×'s, are not excluded by LEP. Although very modest values of F (of order $F \sim 5$) are possible for $m_h < 114$ GeV, the smallest F value found for $m_h \geq 114$ GeV is of order $F \sim 34$, as explained earlier. The increase of the smallest achievable F with m_h is

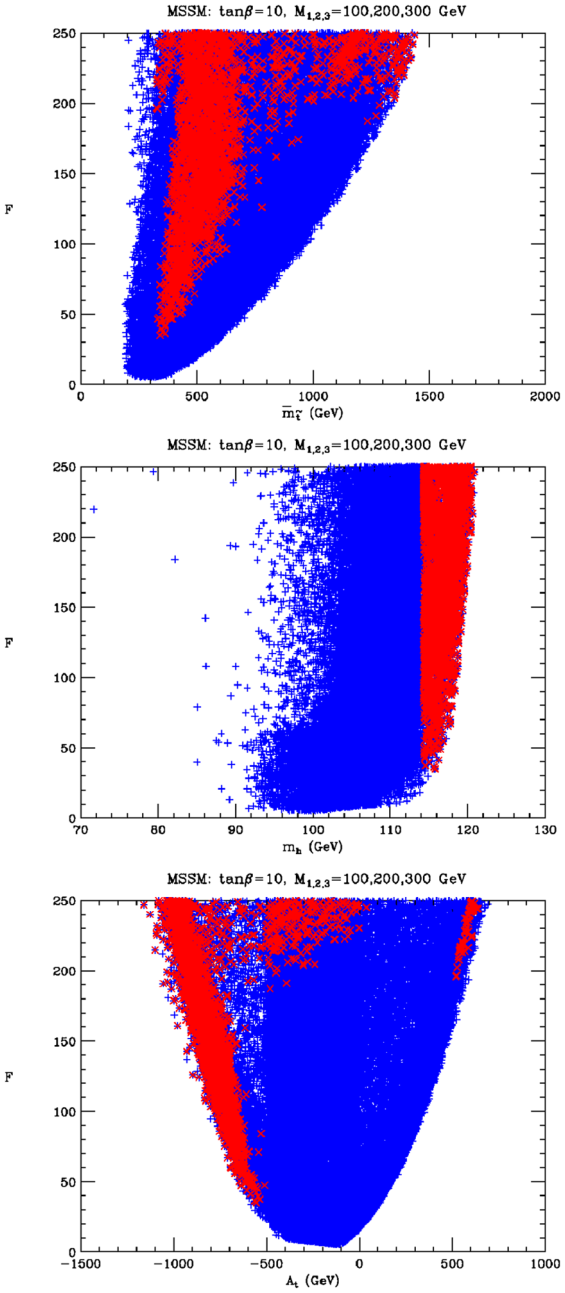

FIG. 2 (color online). Fine-tuning vs $\bar{m}_{\tilde{t}}$ (top), m_h (middle) and A_t (bottom) for randomly generated MSSM parameter choices with $\tan\beta = 10$ and $M_{1,2,3}(m_Z) = 100$, 200, 300 GeV. Blue pluses correspond to parameter choices such that $m_h < 114$ GeV. Red crosses are points with $m_h > 114$ GeV.

illustrated in the middle plot. The modest $F \gtrsim 34$ values are achieved for special parameter choices, namely, $\bar{m}_{\tilde{t}} \sim 300$ GeV and $A_t \sim -500$ GeV corresponding to a large ratio of $A_t/\bar{m}_{\tilde{t}}$; see earlier discussion. A value of $F \sim 34$ corresponds to roughly 3% fine-tuning. Generally speaking, however, it would obviously be nicer if the $m_h \sim 100$ GeV points with $F \sim 5$ were not excluded by LEP.

We now compare these results to what is found in the NMSSM. Plots analogous to those for the MSSM appear in

Fig. 3. Let us first define our conventions (we follow those of Ref. [14]) and discuss a few theoretical points. The superpotential for the Higgs fields is

$$W = \lambda \hat{S} \hat{H}_u \cdot \hat{H}_d + \tfrac{1}{3}\kappa \hat{S}^3, \tag{13}$$

where

$$\hat{H}_u \cdot \hat{H}_d = \hat{H}_u^+ \hat{H}_d^- - \hat{H}_u^0 \hat{H}_d^0. \tag{14}$$

For the soft-SUSY-breaking terms we take

$$V_{\rm soft} = m_{\rm H_u}^2 |H_u|^2 + m_{\rm H_d}^2 |H_d|^2 + m_{\rm S}^2 |S|^2 + (\lambda A_\lambda H_u \cdot H_d S + \tfrac{1}{3}\kappa A_\kappa S^3 + \text{H.c.}). \tag{15}$$

(Above, we have not written the usual terms involving Higgs fields and quark/squark fields.) Assuming that the parameters of the potential are real, W and $V_{\rm soft}$ together yield a full potential for the neutral components of the H_u, H_d, and S scalar fields of the form

$$V = \lambda^2(h_u^2 s^2 + h_d^2 s^2 + h_u^2 h_d^2) + \kappa^2 s^4 + \tfrac{1}{4}\bar{g}^2(h_u^2 - h_d^2)^2 - 2\lambda\kappa h_u h_d s^2 - 2\lambda A_\lambda h_u h_d s + \tfrac{2}{3}\kappa A_\kappa s^3 + m_{H_u}^2 h_u^2 + m_{H_d}^2 h_d^2 + m_S^2 s^2. \tag{16}$$

There are now three minimization conditions

$$\frac{\partial V}{\partial h_u} = 0, \qquad \frac{\partial V}{\partial h_d} = 0, \qquad \frac{\partial V}{\partial s} = 0 \tag{17}$$

which are to be solved for $m_{H_u}^2$, $m_{H_d}^2$ and m_S^2 in terms of the vevs and other parameters appearing in Eq. (16). One combination of the minimization equations yields the MSSM-like expression for m_Z^2 in terms of μ^2, $\tan\beta$, $m_{H_u}^2$ and $m_{H_d}^2$ with μ replaced by $\mu_{\rm eff}$. However, a second combination gives an expression for $\mu_{\rm eff}$ in terms of m_Z and other Higgs potential parameters:

$$\kappa\lambda\left(\frac{1}{\tan\beta} m_{H_d}^2 - m_{H_u}^2 \tan\beta\right) - \lambda^2(m_{H_d}^2 - m_{H_u}^2) = \frac{1}{2} m_Z^2 \frac{\tan^2\beta - 1}{\tan^2\beta + 1}\left[\kappa\lambda\left(\frac{1}{\tan\beta} + \tan\beta\right) - 2\lambda^2 + \frac{2}{\bar{g}^2}\lambda^4\right] + \mu_{\rm eff} A_\lambda \lambda^2\left(\frac{1}{\tan\beta} - \tan\beta\right). \tag{18}$$

Eliminating $\mu_{\rm eff}$, we arrive at an equation of the form $m_Z^4 + B m_Z^2 + C = 0$, with solution $m_Z^2 = -B \pm \sqrt{B^2 - 4C}$, where B and C are given in terms of the soft-SUSY-breaking parameters, λ, κ, and $\tan\beta$. Only one of the solutions to the quadratic equation applies for any given set of parameter choices.

To explore fine-tuning numerically, we proceed analogously to the manner described for the MSSM. At scale m_Z, we fixed $\tan\beta$ and scanned over all allowed values of λ ($\lambda > 0$ by convention and $\lambda \lesssim 0.7$ is required for perturbativity up to the GUT scale) and κ, and over 100 GeV $\leq |\mu_{\rm eff}| \leq 1.5$ TeV, $\text{sign}(\mu_{\rm eff}) = \pm$. We also choose

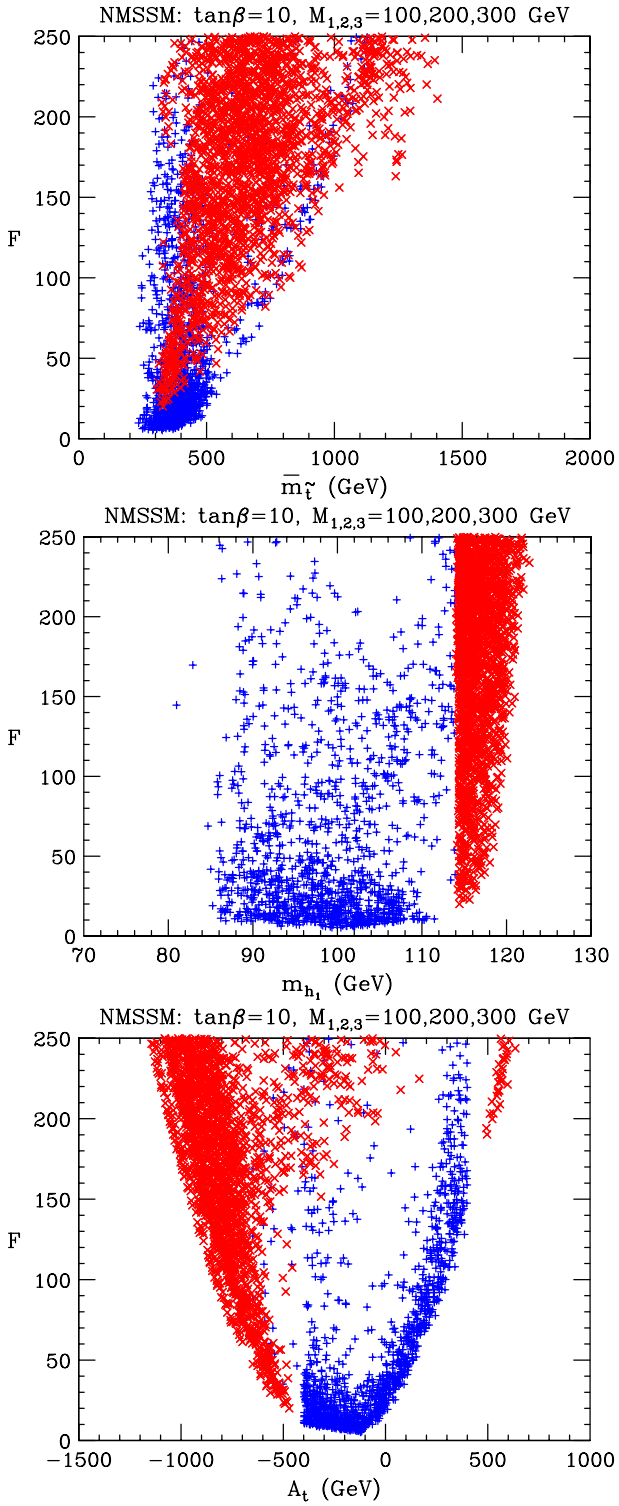

FIG. 3 (color online). For the NMSSM, we plot the fine-tuning measure F vs $\bar{m}_{\tilde{t}}$, m_{h_1} and A_t for NMHDECAY-accepted scenarios with $\tan\beta = 10$ and $M_{1,2,3}(m_Z) = 100$, 200, 300 GeV. Points marked by blue +'s are consistent with LEP limits on the $Z + 2b$ channel and the $Z + 4b$ channel [11], considered separately, *but not necessarily with LEP limits on the combined* $Z + 2b$ *and* $Z + 4b$ *channels*). Points marked by red ×'s escape LEP limits due to $m_{h_1} > 114$ GeV.

m_Z-scale values for the soft-SUSY-breaking parameters A_λ, A_κ, $A_t = A_b$, M_1, M_2, M_3, m_Q^2, m_U^2, m_D^2, m_L^2, and m_E^2, all of which enter into the evolution equations. We process each such choice through NMHDECAY to check that the scenario satisfies all theoretical and experimental constraints, with the exception that we plot some points that are consistent with LEP limits on the $Z + 2b$ and $Z + 4b$ channels considered separately as in [11], but inconsistent with the LEP constraints on the $Z + b's$ final states, where $b's = 2b + 4b$. We shall return to this point shortly. For accepted cases, we then evolve to determine the GUT-scale values of all the above parameters. The fine-tuning derivative for each parameter is determined by shifting the GUT-scale value for that parameter by a small amount, evolving all parameters back down to m_Z, redetermining the potential minimum (which gives new values h_u' and h_d') and finally computing a new value for m_Z^2 using $m_Z'^2 = \bar{g}^2(h_u'^2 + h_d'^2)$.

Our basic results are displayed in Fig. 3. The density of points of a given type should not be taken as having any significance—it simply reflects the nature of the scanning procedures employed for the various cases. In particular, the scans used to obtain results presented in this section were designed to focus on parameter regions with $F < 250$. Further, we focused a lot of our scans on keeping only points with $m_{a_1} < 20$ GeV.

In Fig. 3, one sees a lot of similarity between the NMSSM plots and those for the MSSM, with differences to be noted below. Again, one finds that $F < 10$ (i.e. no worse than 10% fine-tuning of GUT-scale parameters) is easily achieved in the NMSSM for the present modest gluino mass of 300 GeV if the mean stop mass is of order 300–400 GeV which yields $m_{h_1} \sim 100$ GeV (for the case of $\tan\beta = 10$—variation with $\tan\beta$ will be noted later). The associated A_t values are of very modest size, lying in the range $[-400\ \text{GeV}, -100\ \text{GeV}]$. Further, as described in more detail later, the low-F scenarios are once again such that the h_1 is quite SM-like as regards its couplings to WW, ZZ and $f\bar{f}$. The difference between these plots and the earlier MSSM plots is that many (but not all, as we shall explain) of the $m_{h_1} < 114$ GeV points plotted escape all LEP limits. Of course, points with $m_{h_1} > 114$ GeV escape LEP limits simply by being above the maximum LEP-excluded mass.

Let us next discuss in more detail the points with $m_{h_1} < 114$ GeV. They are plotted in Fig. 3 provided that they are consistent with LEP limits on the $Z + 2b$ and $Z + 4b$ channels, considered separately as plotted and tabulated in [11], but not necessarily the combined $Z + b's$ limit. All the plotted $m_{h_1} < 114$ GeV points pass the $Z + 2b$ and $Z + 4b$ separate channel limits by virtue of the fact that $B(h_1 \to a_1 a_1)$ is large enough that $B(h_1 \to b\bar{b})$ is sufficiently suppressed that $Z + h_1 \to Z + b\bar{b}$ lies below the LEP $Z + 2b$ limit, while simultaneously $Z + h_1 \to Z + a_1 a_1 \to b\bar{b}b\bar{b}$ lies below the $Z + 4b$ limit. The values of C_{eff}^{2b} and C_{eff}^{4b} are plotted in Fig. 4 as functions of m_{h_1}. In the C_{eff}^{4b} plot one finds two classes of points with $m_{h_1} < 114$ GeV. The first class has large C_{eff}^{4b} (but still below LEP limits for this individual channel) by virtue of the fact that $B(h_1 \to a_1 a_1)$ is large *and* $m_{a_1} > 2m_b$. The second class of points has zero C_{eff}^{4b} since $m_{a_1} < 2m_b$. F as a function of $B(h_1 \to a_1 a_1)$ is shown in the top plot of Fig. 5.

However, the plotted $m_{h_1} < 114$ GeV points with nonzero C_{eff}^{4b} are mostly not consistent with the LEP data. NMHDECAY allows these points because it does not take into account the need to combine $Z + 2b$ and $Z + 4b$ final states in confronting the LEP limits, which are effectively (at least roughly) on the sum of these two final states. For those $m_{h_1} < 114$ GeV points with nonzero C_{eff}^{4b}, the sum of C_{eff}^{2b} and C_{eff}^{4b} is typically large and one expects such points to have too large a net $Z + b's$ rate, where $b's = 2b + 4b$.

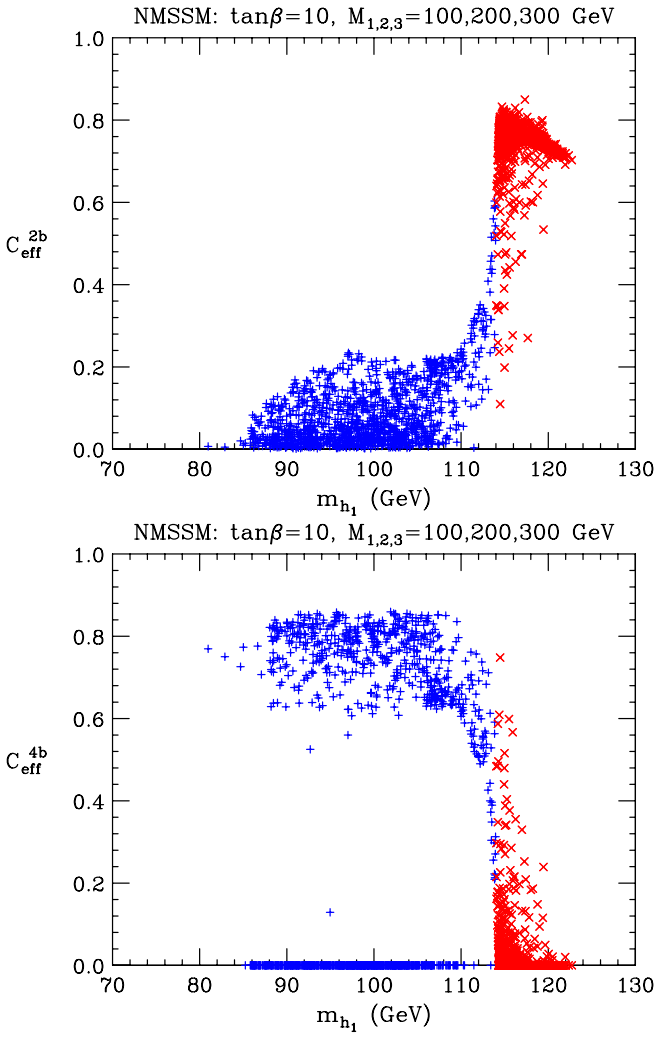

FIG. 4 (color online). For the NMSSM, we plot C_{eff}^{2b} and C_{eff}^{4b} as a functions of m_{h_1} for NMHDECAY-accepted scenarios with $\tan\beta = 10$ and $M_{1,2,3}(m_Z) = 100, 200, 300$ GeV. Point notation as in Fig. 3.

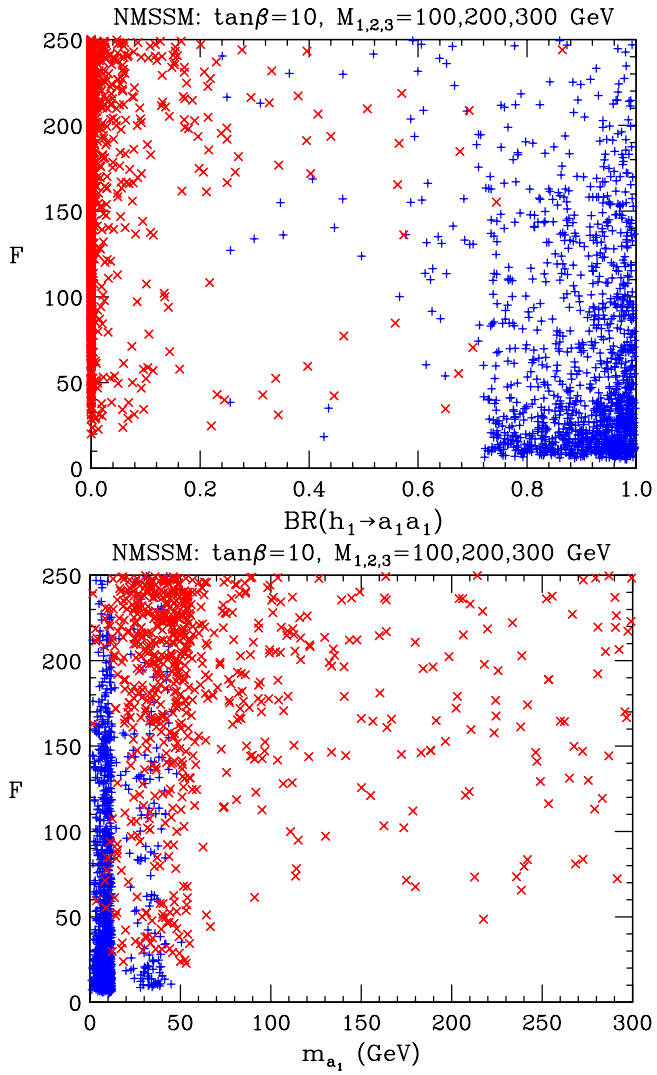

FIG. 5 (color online). For the NMSSM, we plot the fine-tuning measure F vs $BR(h_1 \to a_1 a_1)$ and vs m_{a_1} for NMHDECAY-accepted scenarios with $\tan\beta = 10$ and $M_{1,2,3}(m_Z) = 100$, 200, 300 GeV. Point notation as in Fig. 3.

Indeed, for the limited number of points that were analyzed using the full LEP Higgs working group code one indeed finds [4] that those points with $m_{h_1} \lesssim 110$ GeV that have large $B(h_1 \to a_1 a_1)$ *and* $m_{a_1} > 2m_b$ (implying $a_1 \to b\bar{b}$ predominantly) are inconsistent with LEP limits on the net $Z + b's$ rate. Without analyzing every one of our $m_{a_1} > 2m_b$ points using the full code, we cannot be sure that this same statement applies to all of them.

With this proviso, we thus find that when $m_{h_1} < 114$ GeV, one needs large $B(h_1 \to a_1 a_1)$ *and* $m_{a_1} < 2m_b$ to evade LEP limits. The bottom plot of Fig. 5 shows that it is easy to obtain very low F points that satisfy both criteria. (The less frequent occurrence of $m_{a_1} > 20$ GeV points in this plot is purely an artifact of our scan procedure.) We will turn to a discussion of this in more detail shortly.

As regards $m_{h_1} \geq 114$ GeV points (which are not subject to LEP limits), returning to Fig. 3, we find that F values as low as $\sim$20 (i.e. only 5% tuning of GUT-scale parameters) can be achieved for the special choices of $\bar{m}_{\tilde{t}} \sim 300$ GeV and $A_t \sim -500$ GeV. This is the same region of stop parameter space that yields a minimum $F \sim 34$ with $m_{h_1} > 114$ GeV in the MSSM.

We have also found another type of point with low F and $m_{h_1} \sim 100$ GeV that escapes published LEP limits as follows. First, for these points $B(h_1 \to a_1 a_1)$ is large, $\gtrsim 0.75$, so that $B(h_1 \to b\bar{b}) \lesssim 0.2$, implying a perfectly acceptable LEP rate in the $Zh \to Z2b$ channel. Second, the a_1 is highly singlet and decays mainly into two photons, $B(a_1 \to \gamma\gamma) \gtrsim 0.9$. Thus, there is negligible contribution to the $Zh \to Z4b$ channel. Third, m_{a_1} is typically fairly substantial for these points, $m_{a_1} \sim 30$–45 GeV. However, these points are highly fine-tuned in the sense that the highly singlet nature of the a_1 required for large $B(a_1 \to \gamma\gamma)$ is very sensitive to GUT-scale parameters. This is why they do not appear in the random scans discussed above. Locating such points requires an extremely fine scan over a carefully chosen part of parameter space. We will give more details regarding these points later.

We now briefly describe a third class of points that manage to have relatively low fine-tuning. Generically, in the NMSSM it is easy to have $m_{h_1} < 114$ GeV without violating LEP limits simply by choosing parameters so that the h_1 has substantial singlet S component. In this way, the ZZh_1 coupling is suppressed and the $e^+e^- \to Z^* \to Zh_1$ production rate is reduced to an allowed level even if $h_1 \to b\bar{b}$ decays are dominant. In such scenarios, it is typically the h_2 that is the most SM-like CP-even Higgs boson, but $m_{h_2} > 114$ GeV and LEP constraints do not apply to the h_2. We have performed a broad scan over NMSSM parameter space to look for and investigate the fine-tuning associated with scenarios of this type. We find that not all the points of this type found in our scans are highly fine-tuned. There is a specific parameter region that produces points of this type that are only moderately fine-tuned and for which the h_1 escapes LEP limits by virtue of small ZZh_1 coupling. The lowest F value that we have found for such points is $F \sim 16$. In a separate paper [18], we will describe these scenarios and their fine-tuning in detail and compare to similar MSSM scenarios that are found when $m_A \sim 100$ GeV points are included in the MSSM parameter scans.

III. THE LOW-FINE-TUNING REGION

Armed with this overview, we now return to the parameter region of the NMSSM that allows for the lowest possible fine-tuning, as studied earlier in Sec. II for $\tan\beta = 10$. Here, we consider also $\tan\beta = 3$ and $\tan\beta = 50$. These scans are focused very much on parameter

choices that can yield the lowest F values. The relevant plots are presented in Fig. 6. We present our results in a somewhat different manner than in Sec. II so as to stress the remarkable preference for $m_{h_1} \sim 100$ GeV in order to achieve the very lowest F values at $\tan\beta = 10$, with corresponding preferences for $m_{h_1} \sim 101$ GeV at $\tan\beta = 50$ and $m_{h_1} \sim 90$ GeV at $\tan\beta = 3$. First, we stress that the above m_{h_1} values are the largest ones consistent with low F in an unbiased (i.e. before applying experimental constraints of any kind) scan over the part of parameter space that is simply theoretically consistent (see below). Once one imposes lower bounds on the stop (and chargino) masses, F shows a distinct minimum at the above m_{h_1} values. The preference for these values of m_{h_1} to achieve low F becomes progressively more apparent as one imposes in addition: (a) LEP constraints on Higgs bosons, including the important $Z + 2b$ channel and $Z + 4b$ channels, considered separately (as plotted and tabulated in [11]), but not the combined $Z + 2b$ and $Z + 4b$ channels; and (b) LEP constraints on the combined $Z + 2b$ and $Z + 4b$ channels.

Let us first focus on the $\tan\beta = 10$ case. Four different types of points are displayed. The black crosses show F as a function of m_{h_1} after requiring only that the scenario be theoretically consistent, but before any experimental constraints whatsoever are imposed. The most important components of the theoretical consistency are: (1) that the vacuum corresponds to a proper electroweak symmetry breaking vacuum at a true minimum of the potential; and (2) that the couplings remain perturbative during evolution up to the GUT scale. The black crosses already single out $m_{h_1} \sim 100$ GeV as the point above which F rises rapidly. Black points with low m_{h_1} typically have a rather low value for $m_{\tilde{t}_1}$ that is clearly inconsistent with LEP and Tevatron limits. The minimum F for these low-m_{h_1} black cross points is fairly independent of m_{h_1}. The (green) circles correspond to the black crosses that survive after imposing experimental limits on $m_{\tilde{t}_1}$ and $m_{\tilde{\chi}_1^\pm}$ and similar non-Higgs constraints. We immediately see a striking preference for $m_{h_1} \sim 100$ GeV in order to achieve minimum F. The (blue) squares indicate the points that survive after requiring *in addition* that the scenario be consistent with LEP Higgs limits, including the $Z + 2b$ and $Z + 4b$ final state limits considered separately [11], *but before imposing a limit on the combined* $Z + b's$ ($b's = 2b + 4b$) *final state*. In the case of $\tan\beta = 10$, these blue squares are the union of the $F < 50$ red $\times$'s and blue $+$'s of the middle plot of Fig. 3. The blue-square points now show a very strong preference for $m_{h_1} \sim 100$ GeV, even before, but especially after, focusing on minimal F. The final large (yellow) crosses are the $m_{h_1} < 114$ GeV points among the (blue) square points that have $m_{a_1} < 2m_b$ so that there is no contribution to the $Z + 4b$ channel from the $h_1 \to a_1 a_1$ decay that, in turn, has a sufficiently large branching ratio

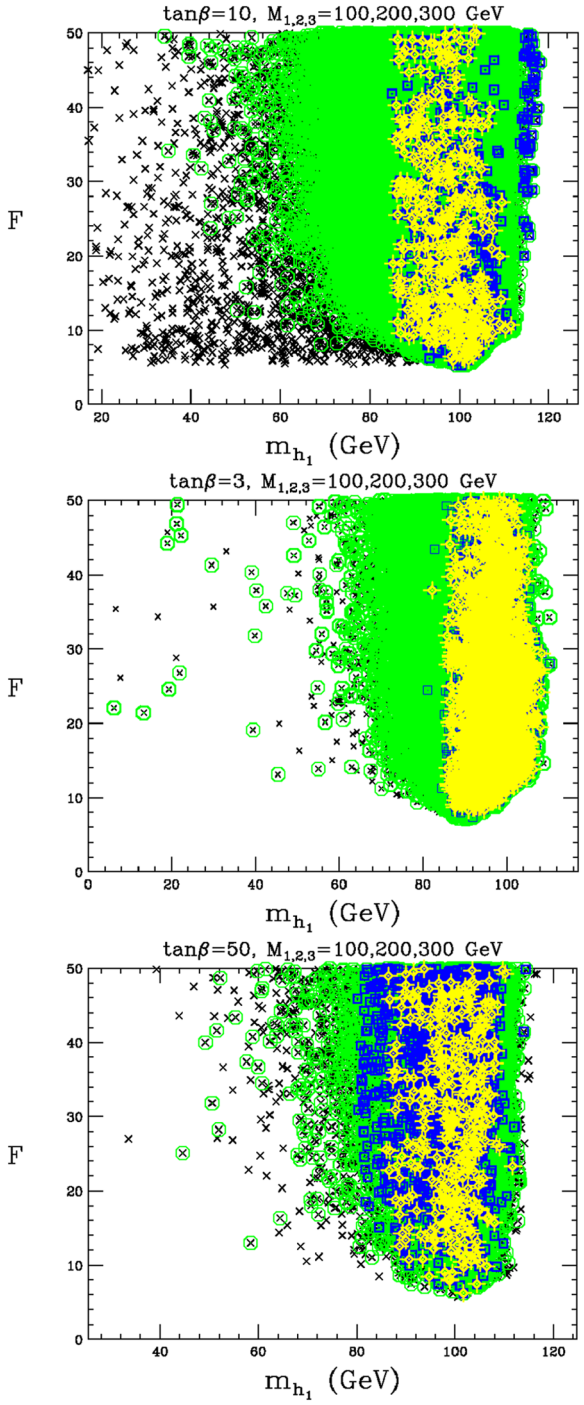

FIG. 6 (color online). Fine-tuning vs m_{h_1} for $\tan\beta = 10$, $\tan\beta = 3$, and $\tan\beta = 50$ for points with $F < 50$, taking $M_{1,2,3}(m_Z) = 100, 200, 300$ GeV. Small black $\times$ points are those obtained after requiring a global and local minimum, no Landau pole before M_U and a neutralino LSP. The green O's are those that in addition satisfy experimental limits on stops and charginos, but not necessarily Higgs limits. The blue $\square$'s are the points that remain after imposing all LEP single channel Higgs limits, in particular, limits [11] on the $Z + 2b$ and $Z + 4b$ channels considered separately. The yellow fancy crosses are the blue square points that remain after requiring $m_{a_1} < 2m_b$, so that LEP limits on $Z + b's$, where $b's = 2b + 4b$, are not violated.

to allow these points to escape the $Z + 2b$ channel LEP limit. Now $m_{h_1} \sim 100$ GeV is clearly singled out.

In the plots for the $\tan\beta = 3$ and $\tan\beta = 50$ cases, we did not bother to generate points with low $m_{\tilde{t}_1}$. So the black cross points in these cases simply indicate the presence of a few scenarios with $m_{\tilde{t}_1}$ above experimental limits but with $m_{\tilde{\chi}_1^\pm}$ below existing limits or some other non-Higgs experimental inconsistency. The green-circle, blue-square, and yellow-cross are as described above.

The large number of blue-square points with very low F indicate that a significant fraction of the very lowest F scenarios are such that h_1 decays primarily into a pair of the lightest CP-odd Higgs bosons of the model, $h_1 \to a_1 a_1$. The yellow crosses show that low-F points with large $B(h_1 \to a_1 a_1)$ *and* $m_{a_1} < 2m_b$ are often found. For such points, $a_1 \to \tau^+\tau^-$ (or $q\bar{q} + gg$ if $m_{a_1} < 2m_\tau$) thereby allowing consistency with LEP constraints on the $Z + b's$ channel and, in many cases, the LEP excess in the $h_1 \to b\bar{b}$ channel for Higgs mass of order 100 GeV.

A. Is small m_{a_1} natural?

Given that low F can be easily achieved without violating LEP constraints if $m_{a_1} < 2m_b$, an important issue is whether obtaining small m_{a_1} requires fine-tuning of GUT-scale parameters. In fact, a light a_1 is natural in the NMSSM in the $A_\kappa, A_\lambda \to 0$ limit. This can be understood as a consequence of a global $U(1)_R$ symmetry of the scalar potential (in the limit $A_\kappa, A_\lambda \to 0$) which is spontaneously broken by the vevs, resulting in a Nambu-Goldstone boson in the spectrum [6,10,20].[2] This symmetry is explicitly broken by the trilinear soft terms so that for small A_κ, A_λ the lightest CP odd Higgs boson is naturally much lighter than other Higgs bosons. In fact, as discussed in depth in [10], the values of A_κ, A_λ needed to have $m_{a_1} < 2m_b$, $B(h_1 \to a_1 a_1) > 0.7$ and low F are quite natural in the context of the NMSSM starting from small or zero values of $A_\kappa(M_U)$ and $A_\lambda(M_U)$. In particular, large $B(h_1 \to a_1 a_1)$ is essentially automatic for typical RGE generated values of A_λ and A_κ ($|A_\kappa(m_Z)| < 10$ GeV and $|A_\lambda(m_Z)| < 200$ GeV) and it is only a question of whether the requirement $m_{a_1} < 2m_b$ is naturally achieved. In [10], we found that essentially no tuning of A_λ and A_κ is required in many model contexts. For example, in the case of $\tan\beta = 10$ tuning of the GUT-scale parameters needed to achieve appropriate A_λ and A_κ is likely to be minimal for scenarios in which the a_1 is about 10% nonsinglet at the state-mixing, amplitude level, i.e. 1% at the probability level.

More precisely, let us define

$$a_1 = \cos\theta_A A_{\rm MSSM} + \sin\theta_A A_S, \tag{19}$$

where $A_{\rm MSSM}$ is the usual two-doublet CP-odd state and A_S is the CP-odd state coming from the S field. Then, the mass of the lightest CP-odd Higgs boson in the simplest approximation is given by:

$$m_{a_1}^2 \simeq 3s\left(\frac{3\lambda A_\lambda \cos^2\theta_A}{2\sin 2\beta} - \kappa A_\kappa \sin^2\theta_A\right). \tag{20}$$

We see that the A_λ contribution to m_{a_1} is suppressed relative to the A_κ contribution for small $\cos\theta_A$ and large $\tan\beta$ and an appropriate balance between the contributions is naturally achieved. In [10], we defined a measure called G that encapsulates the amount of tuning at the GUT scale that is likely to be needed to achieve small m_{a_1}. G is defined using

$$F_{A_\lambda} \equiv \frac{A_\lambda}{m_{a_1}^2}\frac{dm_{a_1}^2}{dA_\lambda}, \qquad F_{A_\kappa} \equiv \frac{A_\kappa}{m_{a_1}^2}\frac{dm_{a_1}^2}{dA_\kappa} \tag{21}$$

as

$$G \equiv \min\{\max[|F_{A_\lambda}|, |F_{A_\kappa}|], |F_{A_\lambda} + F_{A_\kappa}|\}. \tag{22}$$

As shown in [10], small G implies it is quite natural to get small m_{a_1} even for fairly general M_U-scale boundary conditions. For example, if Eq. (20) is approximately correct, so that $m_{a_1}^2$ is linear in A_λ and A_κ, and if A_λ and A_κ are primarily sensitive to a single GUT-scale parameter p, then, if $|F_{A_\lambda} + F_{A_\kappa}|$ is small, sensitivity of $m_{a_1}^2$ to p is guaranteed to cancel. Nonetheless, the measure G should not be overemphasized since specific boundary condition choices can give small m_{a_1} even when G is large.

In Fig. 7, we plot G as a function of $\cos\theta_A$ for parameters choices that yield $F < 15$, taking $\tan\beta = 10$, 3, and 50. The results are displayed using different shadings (colors) for different ranges of m_{a_1}, as delineated in the figure caption. For $\tan\beta = 10$, we see that G is minimal for $|\cos\theta_A| \sim 0.08$, not much above the rough lower bound of $|\cos\theta_A| \sim 0.06$. This lower bound is a direct consequence of the *combined* requirements that: (1) $B(h_1 \to a_1 a_1)$ be so large that $B(h_1 \to b\bar{b})$ is small enough to escape the LEP limit on the $Z + 2b$ channel; and (2) that $m_{a_1} < 2m_b$ so that a_1 does not decay to $b\bar{b}$ and there is no $h_1 \to a_1 a_1 \to b\bar{b}b\bar{b}$ decay contribution to the net $Z + b's$ channel. We also note that small G is only achieved for $m_{a_1} > 2m_\tau$, with $m_{a_1} \gtrsim 7$ GeV preferred.

For $\tan\beta = 3$, there is again a preference for larger m_{a_1} in order to achieve small G. However, small G can be achieved for a much larger range of $\cos\theta_A$. Of course, one should also notice that all the low-F solutions have $\cos\theta_A < 0$, with lower bound of $|\cos\theta_A| \gtrsim 0.06$.

The bottom of the three plots shows that if $\tan\beta = 50$ then it is much more difficult to find solutions with low F that also have low G. The lower bound on $|\cos\theta_A|$ needed to achieve large $B(h_1 \to a_1 a_1)$ shifts downwards slightly to about 0.05.

[2]The alternative for getting a light a_1 is to have a slightly broken Peccei-Quinn symmetry. However, the models with low F are not close to the Peccei-Quinn symmetry limit.

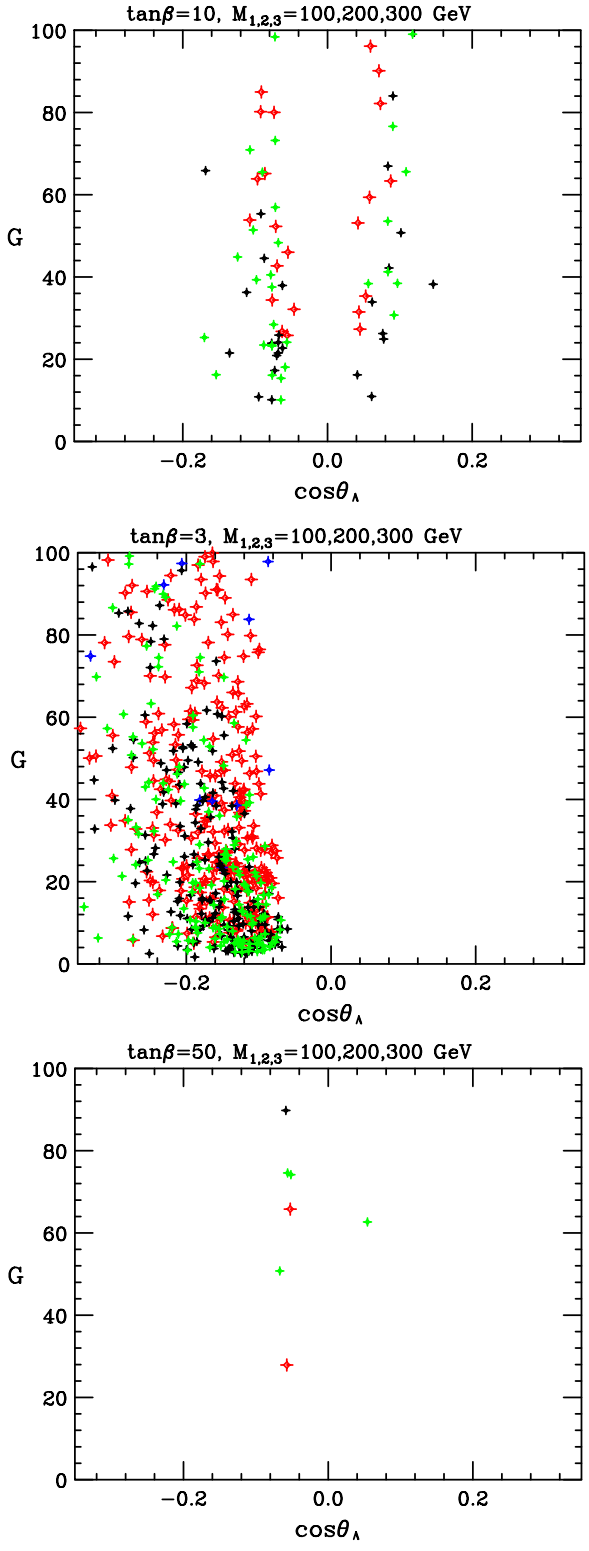

FIG. 7 (color online). For the $F < 15$ scenarios that are fully consistent with all LEP constraints, we plot G vs $\cos\theta_A$ taking $M_{1,2,3} = 100$, 200, 300 GeV and $\tan\beta = 10$ (top), 3 (middle), and 50 (bottom). The point coding is: black = 8.8 GeV $< m_{a_1} < m_{h_1}/2$; dark grey(red) $= 2m_\tau < m_{a_1} <$ 7.5 GeV; light grey(green) $= 7.5$ GeV $< m_{a_1} < 8.8$ GeV; and darkest grey(blue) $= m_{a_1} < 2m_\tau$.

One should note that the coupling of the a_1 to $b\bar{b}$ is proportional to $\tan\beta\cos\theta_A$ times the usual SM-like γ_5 coupling strength. The lower limits on $|\cos\theta_A|$ at $\tan\beta =$ 10, 3, 50 are such that $|\tan\beta\cos\theta_A| \sim 1$, $\sim$0.6, $\sim$2.5. This means that the $b\bar{b}$ coupling is not particularly suppressed, and can even be enhanced with respect to the SM-like γ_5 value. (Of course, the $t\bar{t}$ coupling of the a_1, proportional to $\cot\beta\cos\theta_A$, is very suppressed.) The fact that the $b\bar{b}$ coupling is always significant implies that there is always a significant branching ratio for $\Upsilon \to \gamma a_1$ (where the Υ can be the $1S$, $2S$, or $3S$ state) so long as there is adequate phase space for the decay. The predictions for $B(\Upsilon_{1S} \to \gamma a_1)$ and further discussion appear in [21].

B. Dependence of F on the gluino mass

The minimum value of F that can be achieved is, of course, dependent upon M_3 (and is essentially independent of M_1 and M_2). Indeed, the largest GUT-scale parameter derivative is very frequently that with respect to $M_3(M_U)$. To explore this sensitivity, we have also performed a (somewhat less dense) parameter scan for the case of $M_{1,2,3} = 100$, 200, 600 GeV at $\tan\beta = 10$. The results for F as a function of m_{h_1} are presented in Fig. 8. We find a minimum value of $F \sim 20$ at $m_{h_1} \sim 104$ GeV, the latter being somewhat higher than the $m_{h_1} \sim 100$ GeV location in the corresponding $\tan\beta = 10$, $M_{1,2,3} = 100$, 200, 300 GeV case. A SM-like h_1 with $m_{h_1} \sim 104$ GeV is only consistent with LEP limits if $B(h_1 \to a_1 a_1)$ is large and $m_{a_1} < 2m_b$ [the large (yellow) crosses]. The $m_{h_1} \sim$ 104 GeV location of the minimal F is less consistent with the $M_{2b} \sim 100$ GeV excess in the LEP data. However, to have $m_{h_1} \sim 100$ GeV in the $M_{1,2,3} = 100$, 200, 600 GeV

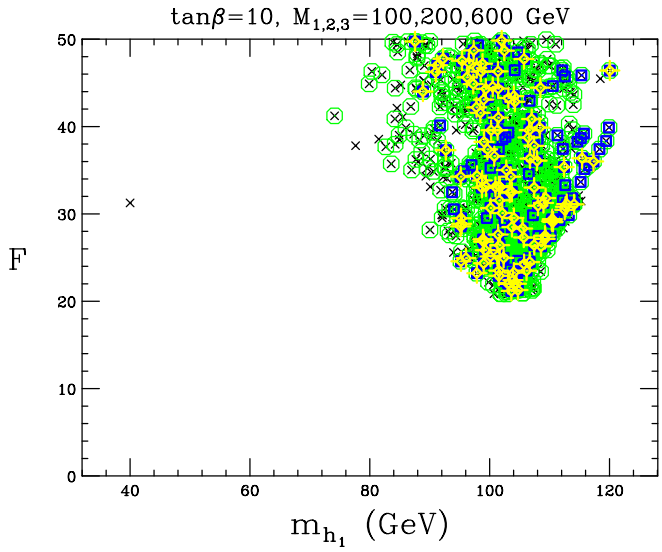

FIG. 8 (color online). Fine-tuning vs the Higgs mass for randomly generated NMSSM parameter choices except for fixed $M_{1,2,3}(m_Z) = 100$, 200, 600 GeV and a fixed value of $\tan\beta = 10$. Notation as in Fig. 6.

case is possible for $F \sim 22$, which is barely different from the $F \sim 20$ minimum value.

One other point of interest is that $m_{a_1} < 2m_b$ points are more easily achieved at larger $m_{h_1} \gtrsim 114$ GeV when $M_3(m_Z) = 600$ GeV than for $M_3(m_Z) = 300$ GeV. This can be understood by considering the special case of $\lambda = 0.2$, $\kappa = \pm 0.2$ and $\tan\beta = 10$. In this case, we find

$$A_\lambda(m_Z) \sim -0.03A_\kappa(M_U) + 0.93A_\lambda(M_U) - 0.35A_t(M_U) - 0.03M_1(M_U) - 0.37M_2(M_U) + 0.66M_3(M_U), \quad (23)$$

$$A_\kappa(m_Z) \sim 0.90A_\kappa(M_U) - 0.11A_\lambda(M_U) + 0.02A_t(M_U) + 0.003M_1(M_U) + 0.025M_2(M_U) - 0.017M_3(M_U). \quad (24)$$

Let us consider the $\kappa > 0$ case (by convention, $\lambda > 0$), for which it can be shown that $A_\kappa < 0$ is required [10] to get $m^2_{a_1} > 0$. From Eqs. (7), (8), and (24), one finds that $A_\kappa(m_Z) \sim 0.06M_3(m_Z) + 0.1A_t(m_Z)$, implying that increasingly negative $A_t(m_Z)$ is required to achieve $A_\kappa < 0$ as $M_3(m_Z)$ increases. From Eq. (20), a small value of $m^2_{a_1}$ will be easily achieved in the present case of $\kappa A_\kappa < 0$ if $A_\lambda(m_Z) < 0$ so that the $\kappa A_\kappa(m_Z)$ and $\lambda A_\lambda(m_Z)$ terms tend to cancel. Equations (7), (8), and (23) imply $A_\lambda(m_Z) \sim -0.3M_3(m_Z) - 1.5A_t(m_Z)$ which gives $A_\lambda(m_Z) < 0$ for increasingly negative $A_t(m_Z)$ as $M_3(m_Z)$ increases. In short, the larger $M_3(m_Z)$ is the more negative $A_t(m_Z)$ can be while requiring small $m^2_{a_1}$. The more negative $A_t(m_Z)$, the larger stop mixing is at fixed $\bar{m}_{\tilde{t}}$ and therefore the larger m_{h_1}.

C. Low-F scenarios and the LEP excess

We will now discuss in more detail other properties of the low-F scenarios with $m_{h_1} \sim 100$ GeV and $m_{a_1} < 2m_b$, focusing first on the case of $\tan\beta = 10$ and $M_{1,2,3}(m_Z) = 100, 200, 300$ GeV. First, we recall our earlier results from [3]. There, we studied in detail the $F < 25$ points from our earliest $\tan\beta = 10$ scans as plotted in Fig. 1. The plot shows the $C^{2b}_{\rm eff}$ predictions for all parameter choices in our scan that had $F < 25$ and $m_{a_1} < 2m_b$ and that are consistent with the experimental and theoretical constraints built into NMHDECAY as well as with limits from the preliminary LHWG full analysis code [4], which, in particular, incorporates limits on the $Z + b's$ combined channel. Eight $F < 10$ points are singled out. As we have emphasized, these latter points cluster near $m_{h_1} \sim 98$–105 GeV. In [3], we found the remarkable result that not only are these $F < 10$ $m_{a_1} < 2m_b$ points consistent with LEP limits, but also most are such that m_{h_1} and $B(h_1 \to b\bar{b})$ are appropriate for explaining the $C^{2b}_{\rm eff}$ excess. We wish to emphasize that in our scan there are many, many points that satisfy all constraints and have $m_{a_1} < 2m_b$. The remarkable result is that those with $F < 10$ have a substantial probability that they predict the Higgs boson properties that would imply a LEP $Zh \to Z + b$'s excess of the sort seen. We stress again that the $F < 10$ points with m_{a_1} substantially above $2m_b$ all predict a net $Z + b$'s signal that is ruled out at better than 99% CL by LEP data. Indeed, all such $F < 25$ points have a net $h_1 \to b$'s branching ratio, $B(h_1 \to b\bar{b}) + B(h_1 \to a_1a_1 \to b\bar{b}b\bar{b}) \gtrsim 0.85$, which is too large for LEP consistency. In our larger scans, as represented by the $C^{2b}_{\rm eff}$ results of Fig. 4, we see a huge number of $m_{a_1} < 2m_b$ points with approximately the correct $C^{2b}_{\rm eff}$ to explain the LEP 100 GeV excess.

For $\tan\beta = 50$, $M_{1,2,3}(m_Z) = 100, 200, 300$ GeV, the preference for $m_{h_1} \sim 101$ GeV to achieve low F will again imply that many of the lowest F scenarios will provide a natural explanation of the $Z + 2b$ LEP excess. At $\tan\beta = 3$, the very lowest F values, $F \sim 7$–8, consistent with LEP limits are achieved for $m_{h_1} \sim 95$ GeV, as shown in the middle plot of Fig. 6. Such an h_1 mass is too low to provide a natural explanation of the $Z + 2b$ excess. However, this same plot shows that the very slightly higher value of $F \sim 10$ is possible for $m_{h_1} \sim 100$ GeV. Thus, the LEP $Z + 2b$ excess is fully consistent with low fine-tuning scenarios that pass all LEP Higgs limits for all $\tan\beta \geq 3$. (We have not explored still lower values.) Of course, it is equally true that at $\tan\beta = 10$ and $\tan\beta = 50$, only a very modest increase in F would be needed for m_{h_1} to take on a value that is not perfectly correlated with the location at $M_{2b} \sim 100$ GeV of the $Z + 2b$ LEP excess.

D. Properties of the heavier Higgs bosons for low-F scenarios

Another interesting question is whether there is any correlation between F and m_{a_1} or between F and the masses of the heavier Higgs bosons, m_{h^+}, m_{a_2}, m_{h_2}, and m_{h_3}. The plots for $\tan\beta = 10$ appear in Figs. 9 and 10. There, we observe that F depends very weakly on m_{a_1} (once $m_{a_1} < 2m_b$), but that lower values of m_{h^+}, m_{a_2}, m_{h_2}, m_{h_3} are definitely preferred to obtain small F and that to obtain fully allowed yellow fancy crosses with $F < 10$ requires $m_{h^+} \in [300\ \text{GeV}, 800\ \text{GeV}]$, $m_{a_2} \in [250\ \text{GeV}, 750\ \text{GeV}]$, $m_{h_2} \in [200\ \text{GeV}, 600\ \text{GeV}]$ and $m_{h_3} \in [300\ \text{GeV}, 800\ \text{GeV}]$. The corresponding plots for $\tan\beta = 50$ appear in Figs. 11 and 12. Again, we observe that F depends very weakly on m_{a_1}, and that lower values of m_{h^+}, m_{a_2}, m_{h_2}, m_{h_3} are definitely preferred to obtain small F. For $\tan\beta = 50$, to obtain fully allowed yellow fancy crosses with $F < 10$ requires $m_{h^+} \in [250\ \text{GeV}, 750\ \text{GeV}]$, $m_{a_2} \in [250\ \text{GeV}, 750\ \text{GeV}]$, $m_{h_2} \in [200\ \text{GeV}, 650\ \text{GeV}]$, and $m_{h_3} \in [250\ \text{GeV}, 750\ \text{GeV}]$.

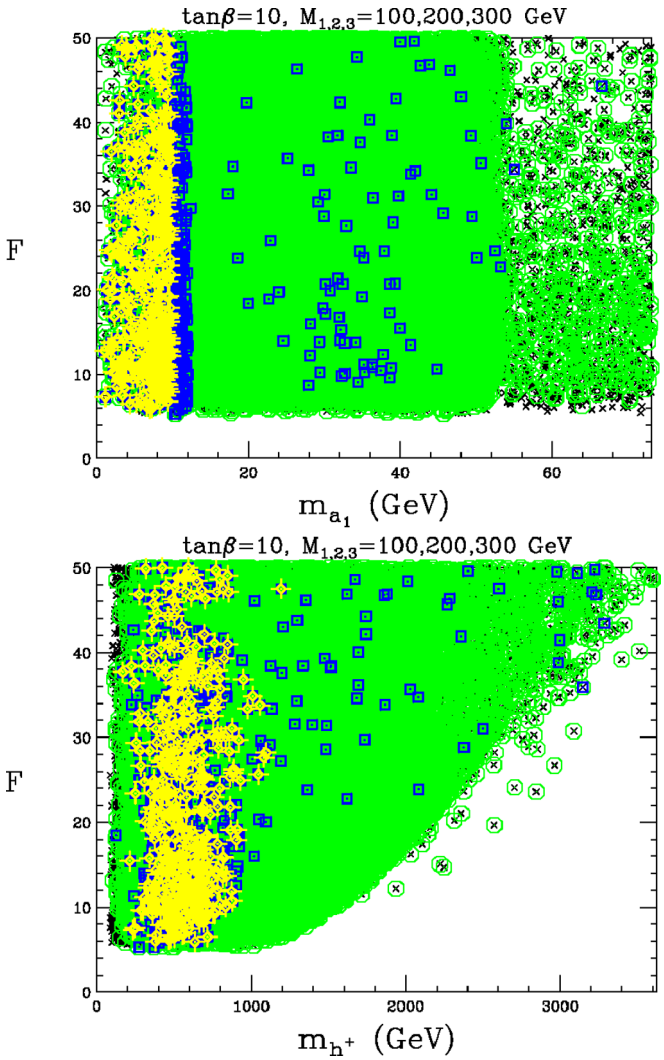

FIG. 9 (color online). Fine-tuning vs m_{a_1} (top) and vs m_{h^+} (bottom) for points with $F < 50$ taking $M_{1,2,3}(m_Z) = 100$, 200, 300 GeV and $\tan\beta = 10$. Point notation as in Fig. 6.

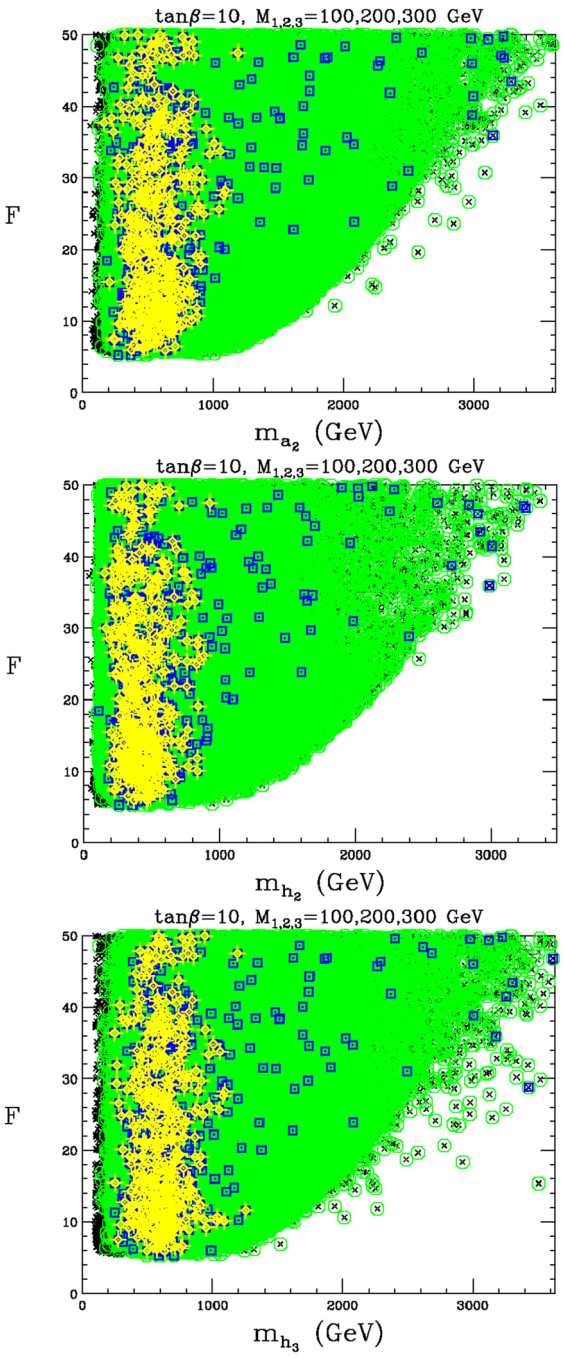

FIG. 10 (color online). Fine-tuning vs m_{a_2} (top), m_{h_2} (middle), and m_{h_3} (bottom) for points with $F < 50$ taking $M_{1,2,3}(m_Z) = 100$, 200, 300 GeV and $\tan\beta = 10$. Point notation as in Fig. 6.

These results have implications for the LHC and ILC. At the LHC, the main processes for producing and detecting these heavier Higgs bosons are $gg \to b\bar{b}H$ (where $H = a_2$, h_2, h_3) and $gg \to b\bar{t}h^+ + gg \to \bar{b}th^-$, with, for example, $H \to \tau^+\tau^-$. One finds [22] that detection becomes possible when the $b\bar{b}H$ and $b\bar{t}h^+$ couplings are enhanced by large $\tan\beta$. The mass ranges for the heavier Higgs bosons preferred for obtaining low F are such that if $\tan\beta = 10$ they will be on the margin of detectability at the LHC, whereas if $\tan\beta = 50$ they will certainly be detectable. (At $\tan\beta = 3$ the small-F mass ranges for the h_2, h_3, a_2 are similar, but $\tan\beta$ is definitely too small for the above LHC modes to be detectable.) For the lowest part of the mass ranges, a signal for $gg \to b\bar{b}H$ might also emerge at the Tevatron if $\tan\beta = 50$. It is also important to note that the low-F mass ranges of the a_2, h_2, h_3, h^+ are such that their pair production would mostly be outside the kinematical reach of a $\sqrt{s} = 500$ GeV ILC, but that a substantial portion of the mass ranges are such that pair production would be possible at a $\sqrt{s} = 1$ TeV ILC.

E. Features and parameter correlations for low-F scenarios

We next turn to a detailed discussion of various correlations among the NMSSM parameters that are associated with low-F scenarios having large $B(h_1 \to a_1 a_1)$ and

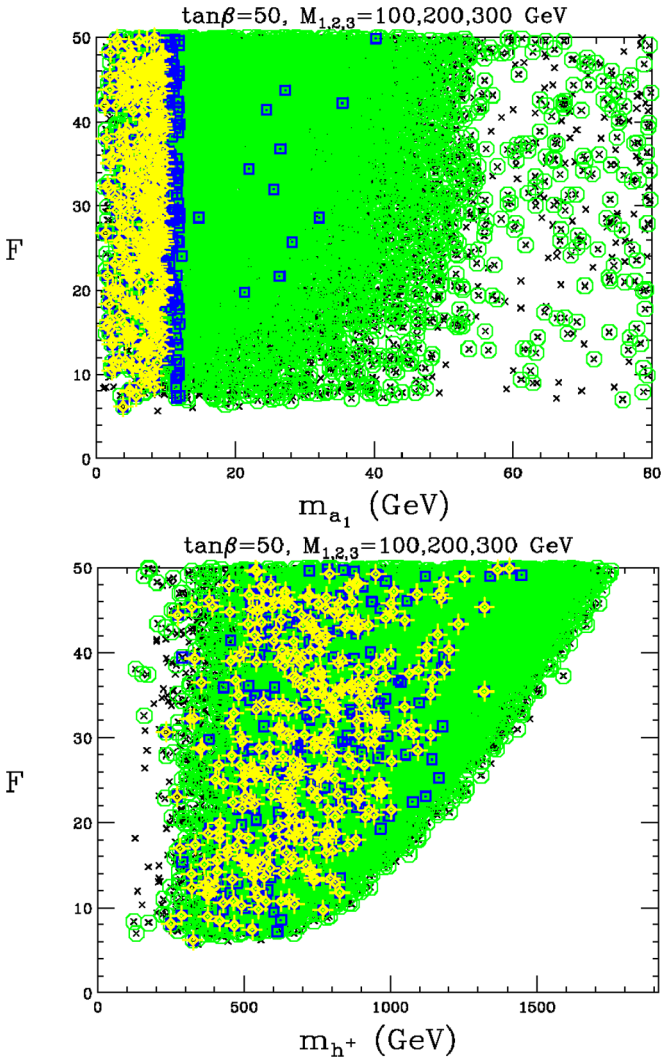

FIG. 11 (color online). Fine-tuning vs m_{a_1} (top) and vs m_{h^+} (bottom) for points with $F < 50$ taking $M_{1,2,3}(m_Z) = 100$, 200, 300 GeV and $\tan\beta = 50$. Point notation as in Fig. 6.

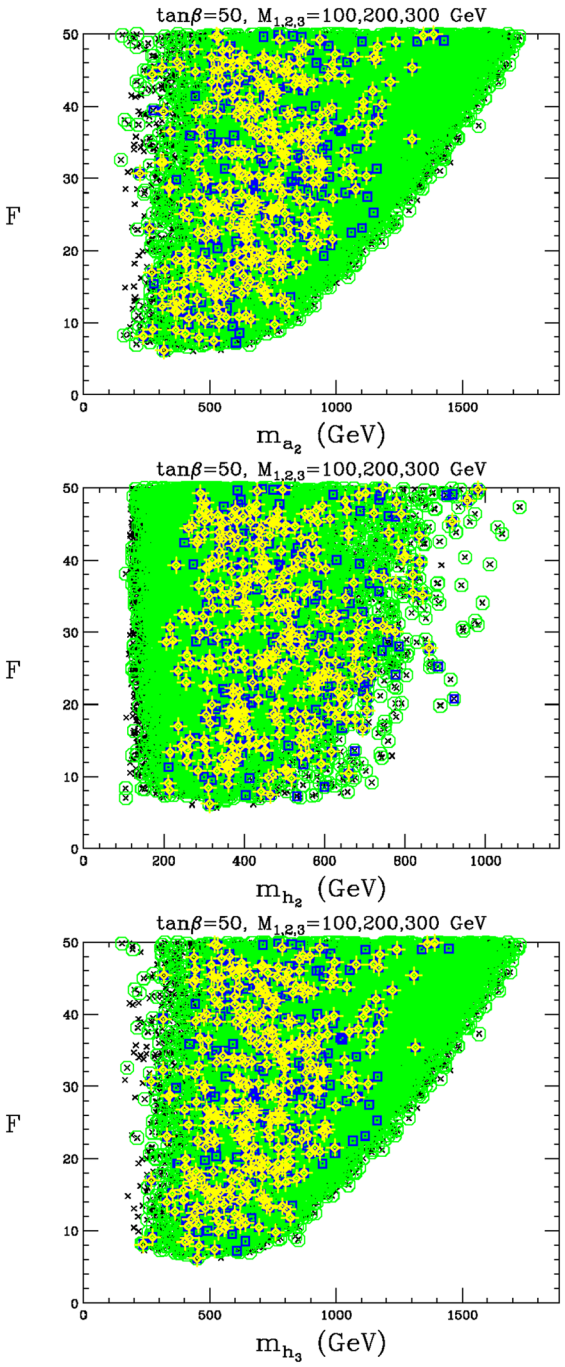

FIG. 12 (color online). Fine-tuning vs m_{a_2} (top), m_{h_2} (middle), and m_{h_3} (bottom) for points with $F < 50$ taking $M_{1,2,3}(m_Z) = 100$, 200, 300 GeV and $\tan\beta = 50$. Point notation as in Fig. 6.

$m_{a_1} < 2m_b$, i.e. the points indicated by the large yellow crosses in the previous figures. We call such points "fully okay." We first present some figures to illustrate how the fully okay points compare to points that are either experimentally excluded or else have sufficiently large m_{h_1} (roughly $m_{h_1} > 110$–114 GeV) as to avoid LEP constraints on the $Z + b's$ channel. These latter points are the (blue) squares, (green) circles and black $\times$'s of the earlier plots.

First consider A_t. Plots of F as a function of $A_t(m_Z)$ and $A_t(M_U)$ are given in Figs. 13 and 14 for $\tan\beta = 10$ and $\tan\beta = 50$, respectively. These show that rather well-defined (and rather $\tan\beta$-independent) values are needed to achieve the very lowest F values, especially after imposing Higgs boson experimental limits. At scale m_Z the preferred $A_t(m_Z)$ is of order -100 GeV. The corresponding $A_t(M_U)$ is of order $+600$ GeV. The lowest F values are of course those associated with $m_{h_1} \sim 100$ GeV. This is consistent with our earlier discussion. The $\tan\beta = 10$ points with large negative $A_t(m_Z)$ values that escape LEP limits by virtue of $m_{h_1} > 114$ GeV are the dark (blue) squares that begin at $F \sim 20$ and $A_t(m_Z) \sim -500$ GeV.

In Figs. 15 and 16, we plot F as a function of $\mu_{\rm eff}$ (which in the case of the NMSSM is only defined at scale m_Z where electroweak symmetry breaking has occurred) for the cases of $\tan\beta = 10$ and $\tan\beta = 50$, respectively. As

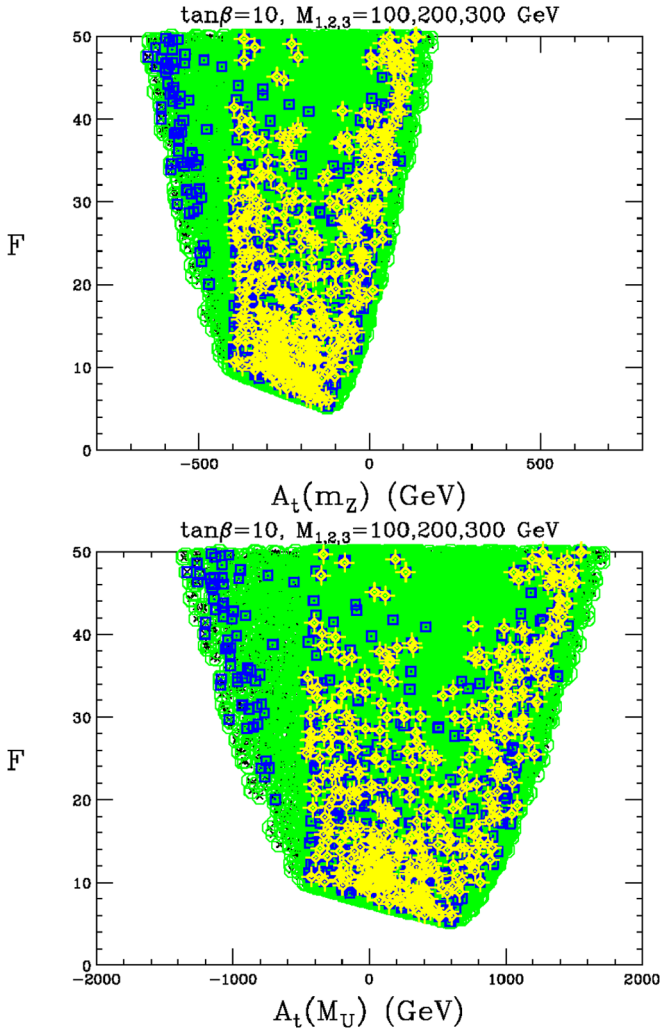

FIG. 13 (color online). Fine-tuning vs $A_t(m_Z)$ (top) and vs $A_t(M_U)$ (bottom) for points with $F < 50$ taking $M_{1,2,3}(m_Z) = 100$, 200, 300 GeV and $\tan\beta = 10$. Point notation as in Fig. 6.

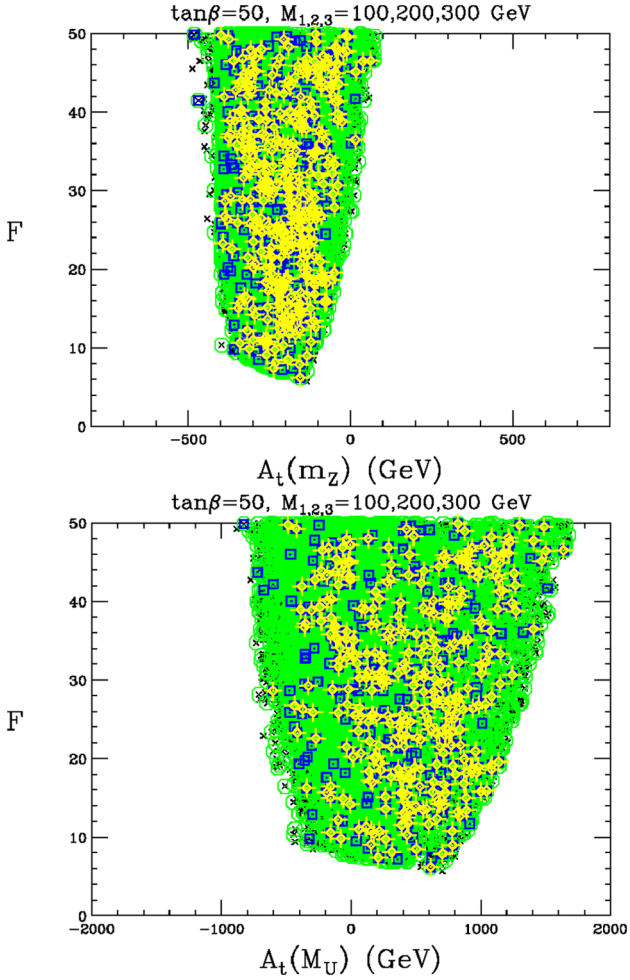

FIG. 14 (color online). Fine-tuning vs $A_t(m_Z)$ (top) and vs $A_t(M_U)$ (bottom) for points with $F < 50$ taking $M_{1,2,3}(m_Z) = 100$, 200, 300 GeV and $\tan\beta = 50$. Point notation as in Fig. 6.

one could easily anticipate from Eq. (5) (with μ replaced by $\mu_{\rm eff}$), fine-tuning is smallest for the smallest values of $\mu_{\rm eff}$. This figure also shows that $|\mu_{\rm eff}|$ values below about 100 GeV are eliminated by the LEP limit on the mass of the lightest chargino.

Next, let us examine the soft squark masses—M_Q, M_U, and M_D—of the third generation. Values for these at scale m_Z are plotted in Figs. 17 and 18 for $\tan\beta = 10$ and $\tan\beta = 50$, respectively. We see that to obey limits on stop masses, there is a fairly definite lower bound on $M_Q(m_Z)$ and $M_D(m_Z)$, although low values for $M_U(m_Z)$ are possible. And, to achieve $F < 15$ and satisfy all experimental limits requires all these soft masses to lie in a very well-defined band. The corresponding GUT-scale values are given in Figs. 19 and 20. Points with $F < 15$ satisfying all limits again have soft masses squared at the GUT scale that fall within narrow bands (and are sometimes negative and sometimes positive).

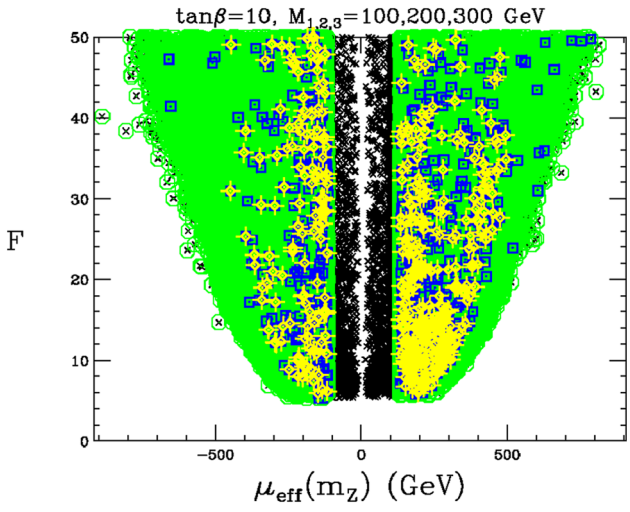

FIG. 15 (color online). Fine-tuning vs $\mu_{\rm eff}$ for points with $F < 50$ taking $M_{1,2,3}(m_Z) = 100$, 200, 300 GeV and $\tan\beta = 10$. Point notation as in Fig. 6.

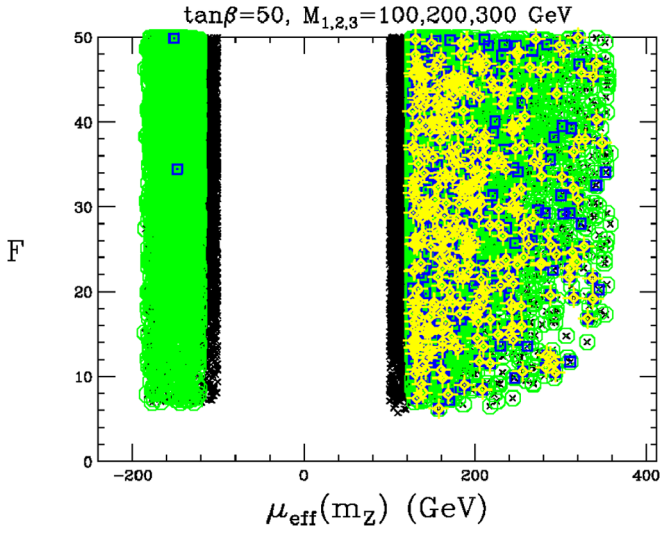

FIG. 16 (color online). Fine-tuning vs $\mu_{\rm eff}$ for points with $F < 50$ taking $M_{1,2,3}(m_Z) = 100, 200, 300$ GeV and $\tan\beta = 50$. Point notation as in Fig. 6.

Next, we examine, for the case of $\tan\beta = 10$, A_λ and A_κ at scale m_Z. Figure 21 gives some results. The upper plot shows that $F < 15$ can be achieved for a wide range of $A_\lambda(m_Z)$, with points that obey all limits requiring a minimum value of $|A_\lambda(m_Z)| \gtrsim 40$ GeV. The middle plot shows that fully okay points require $A_\kappa(m_Z)$ in a rather narrow band with $0.8 < |A_\kappa(m_Z)| < 15$. The bottom plot shows the correlation between $A_\kappa(m_Z)$ and $A_\lambda(m_Z)$ that is required to get small $m_{a_1} < 2m_b$, as discussed earlier. Note that either both must be negative or both positive for any point that is fully consistent with experimental limits. The lower bounds on their absolute values for the fully okay points—the large yellow crosses—are those required to have large enough $B(h_1 \to a_1 a_1)$ to escape the $Z + b's$ LEP limits for $m_{h_1} \sim 100$ GeV. Similar results are obtained for $\tan\beta = 50$. All these results can be understood analytically as discussed in [10].

Figure 22 shows the dependence on m_{a_1} on $A_\lambda(m_Z)$ and $A_\kappa(m_Z)$ in the case of $\tan\beta = 10$. One observes that large m_{a_1} can be achieved for these same ranges of $A_\lambda(m_Z)$ and $A_\kappa(m_Z)$ just as easily as small m_{a_1}. It is just that cases with large $m_{a_1} > 2m_b$ and small F, which requires $m_{h_1} \sim 100$ GeV, are not consistent with LEP limits on the net $Z + b's$ channel, as we have discussed. Similar results are found for $\tan\beta = 50$.

Plots of the GUT-scale parameters, $A_\lambda(M_U)$ and $A_\kappa(M_U)$, appear in Fig. 23. These show that the lowest-F scenarios that are fully consistent with experiment are often achieved for small values of these parameters. In terms of model building, these soft-SUSY-breaking parameters are thus close to values associated with "no-scale" soft-SUSY-breaking.

Probably the most interesting parameter correlation is that regarding the soft-SUSY-breaking Higgs masses squared at the GUT scale. These are plotted in Figs. 24 and 25 for the cases of $\tan\beta = 10$ and $\tan\beta = 50$, respectively. These plots show that the fully okay scenarios with smallest F have very modest soft masses squared at the GUT scale, especially in the case of $m^2_{H_u}$. Thus, something close to a "no-scale" model for soft Higgs masses squared at the GUT scale is preferred for low F.

This preference for a "no-scale" type of boundary condition for the Higgs soft masses squared at the GUT scale is

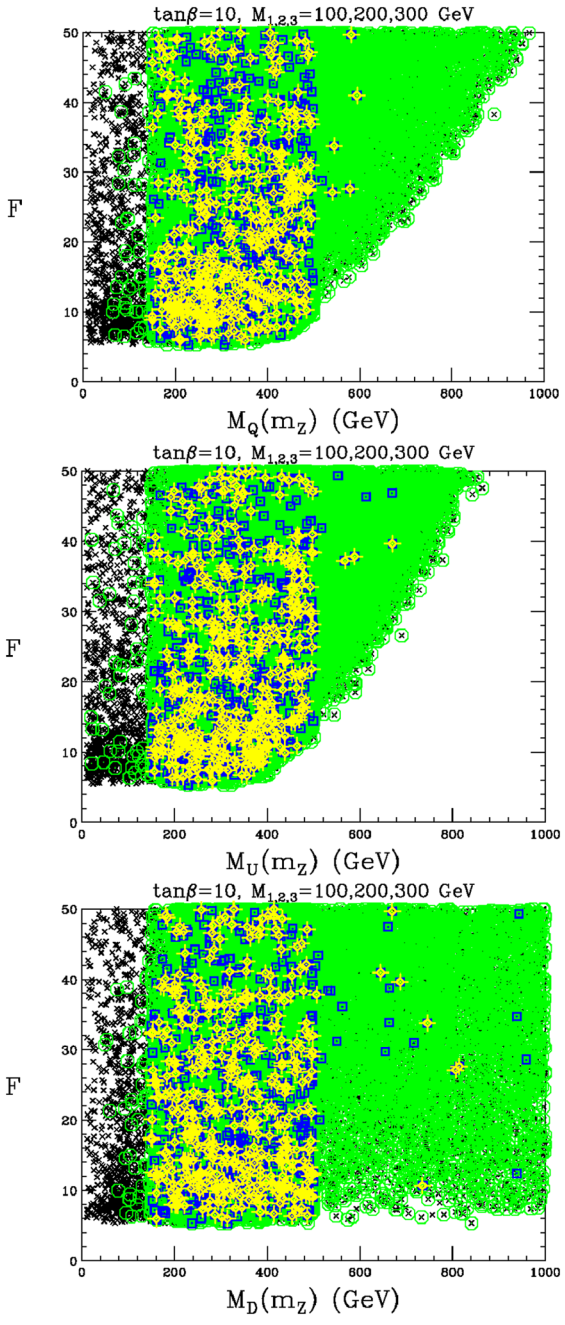

FIG. 17 (color online). Fine-tuning vs $M_Q(m_Z)$, $M_U(m_Z)$, and $M_D(m_Z)$ for points with $F < 50$ taking $M_{1,2,3}(m_Z) = 100$, 200, 300 GeV and $\tan\beta = 10$. Point notation as in Fig. 6.

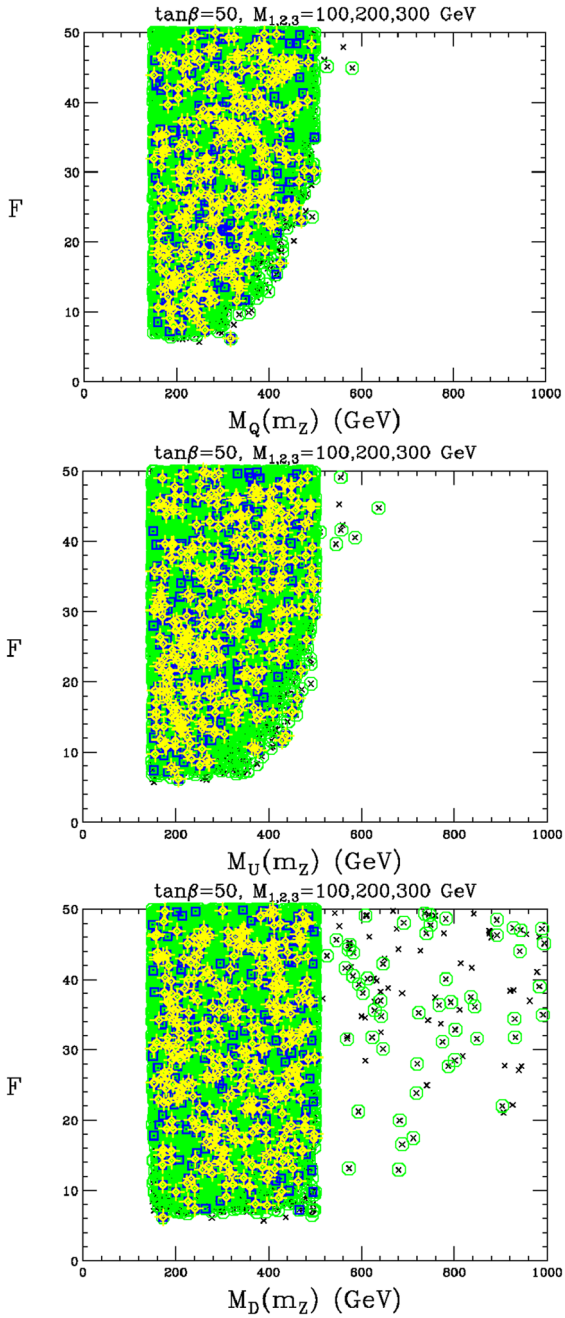

FIG. 18 (color online). Fine-tuning vs $M_Q(m_Z)$, $M_U(m_Z)$, and $M_D(m_Z)$ for points with $F < 50$ taking $M_{1,2,3}(m_Z) = 100$, 200, 300 GeV and $\tan\beta = 50$. Point notation as in Fig. 6.

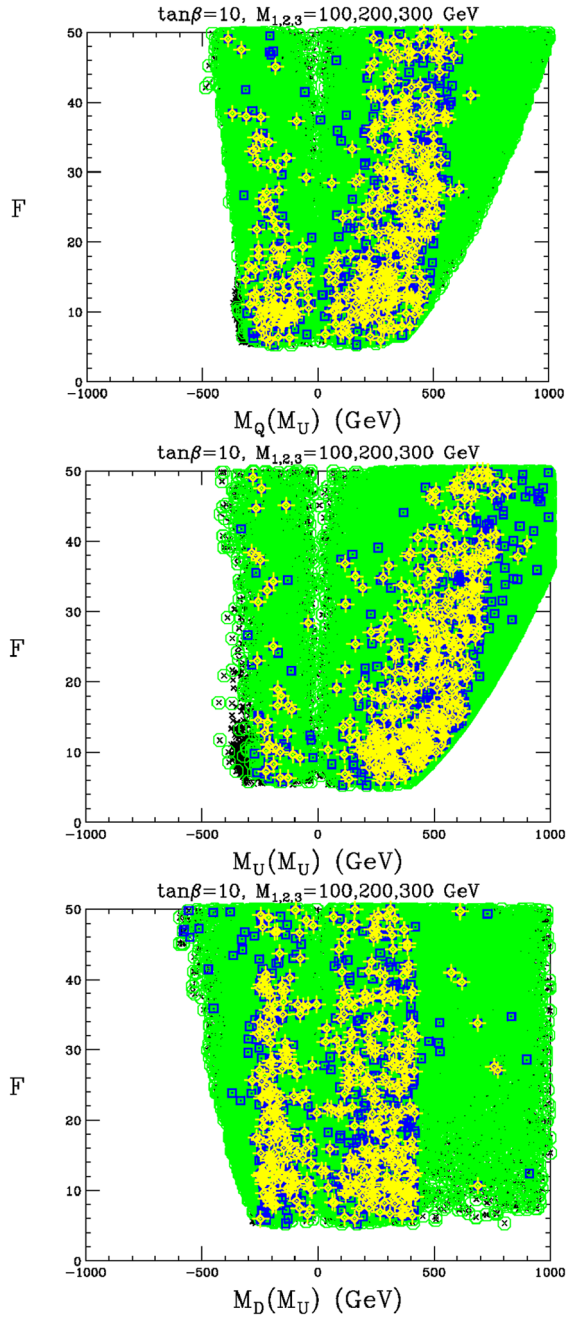

FIG. 19 (color online). Fine-tuning vs $M_Q(M_U)$, $M_U(M_U)$, and $M_D(M_U)$ for points with $F < 50$ taking $M_{1,2,3}(m_Z) = 100$, 200, 300 GeV and $\tan\beta = 10$. Point notation as in Fig. 6. Negative values indicate cases for which $M^2_{Q,U,D} < 0$ in which case the plot gives $-\sqrt{-M^2_{Q,U,D}}$.

further emphasized by the $\tan\beta = 10$ plot of Fig. 26, where we overlap the values of $m^2_{H_u}(M_U)$, $m^2_{H_d}(M_U)$ and $m^2_S(M_U)$ for $F < 50$ yellow fancy cross scenarios of Fig. 24.

We have said in many places that for the fully okay scenarios the h_1 has quite SM-like h_1ZZ coupling. This is illustrated in Fig. 27 where we plot F as a function of

$$C_V \equiv \frac{g_{h_1ZZ}}{g_{h_{\rm SM}ZZ}}, \tag{25}$$

for the case of $\tan\beta = 10$ (results for $\tan\beta = 50$ are similar). We see that the fully okay yellow fancy crosses all have $|C_V| \sim 1$. In fact, for $F < 50$ scenarios, $|C_V| \sim 1$ also for the (blue) square points that are not also yellow fancy crosses, i.e. those points obtained if one only requires that the scenario is consistent with experimental limits that include the $Z + 2b$ channel (that is, before requiring $m_{a_1} < 2m_b$ as needed to avoid the limits on the combined $Z + b's$

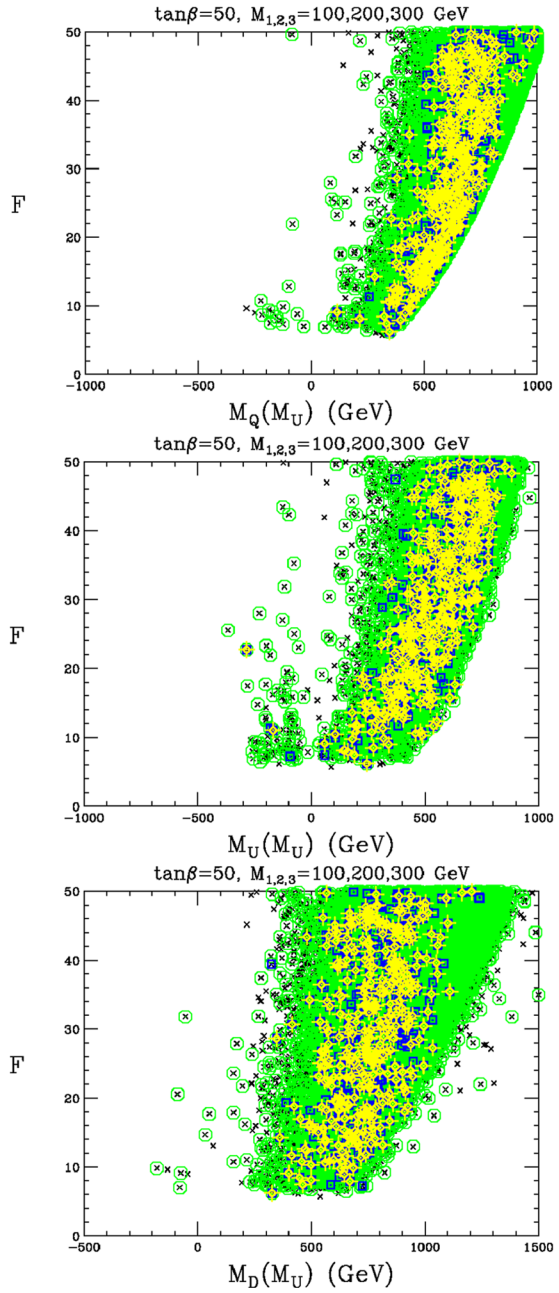

FIG. 20 (color online). Fine-tuning vs $M_Q(M_U)$, $M_U(M_U)$, and $M_D(M_U)$ for points with $F < 50$ taking $M_{1,2,3}(m_Z) = 100$, 200, 300 GeV and $\tan\beta = 50$. Point notation as in Fig. 6. Negative values indicate cases for which $M^2_{Q,U,D} < 0$ in which case the plot gives $-\sqrt{-M^2_{Q,U,D}}$.

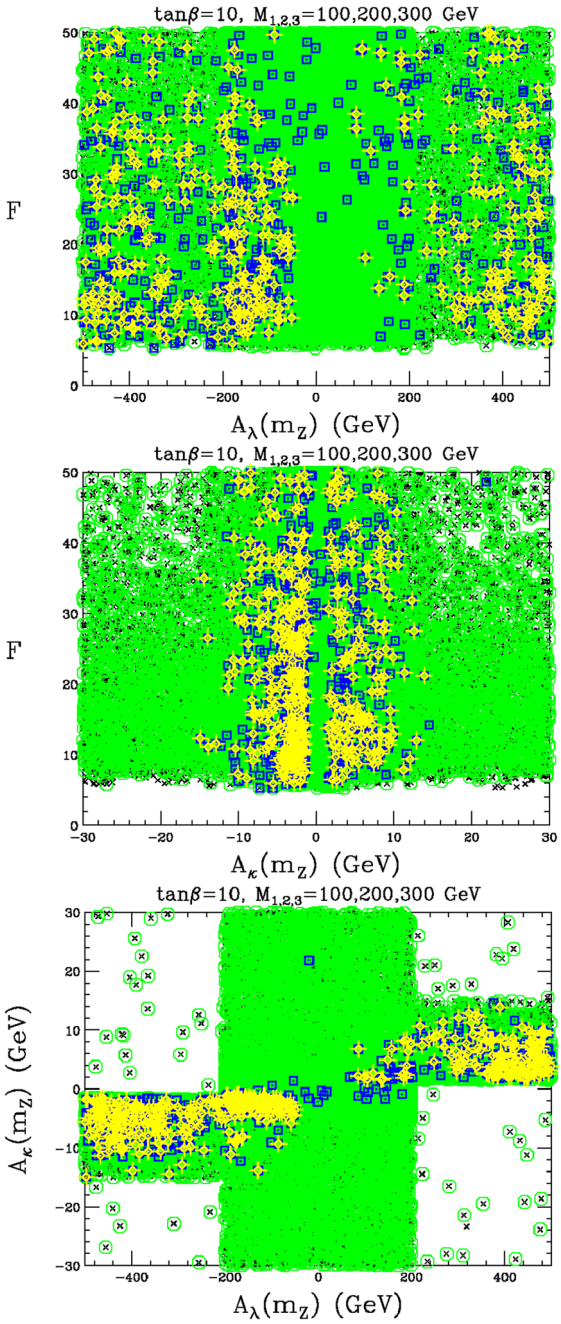

FIG. 21 (color online). F vs $A_\lambda(m_Z)$ and $A_\kappa(m_Z)$ (upper two plots) and $A_\kappa(m_Z)$ vs $A_\lambda(m_Z)$ (lower plot) for points with $F < 50$ taking $M_{1,2,3}(m_Z) = 100$, 200, 300 GeV and $\tan\beta = 10$. Point notation as in Fig. 6.

channel). Suppressed $|C_V|$ values only appear in these plots if the Higgs experimental limits are removed. As discussed later, there are some very special points for which this is not true that will be considered in a follow-up paper.

F. Parameter correlations for the very lowest F points

In this subsection, we consider at a still more detailed level the fully okay yellow points having large $B(h_1 \to a_1 a_1)$ and $m_{a_1} < 2m_b$ that also have $F < 10$. We will present results only for the case of $\tan\beta = 10$ and M_1, M_2, $M_3 = 100$, 200, 300 GeV. In general, the other $\tan\beta$ values give similar correlations aside from the shift in the value of m_{h_1} that gives the lowest F value. In the plots presented in this section we will use blue $+$'s in place of the yellow crosses, since the latter do not display well on their own. Hopefully, there are few enough points on the

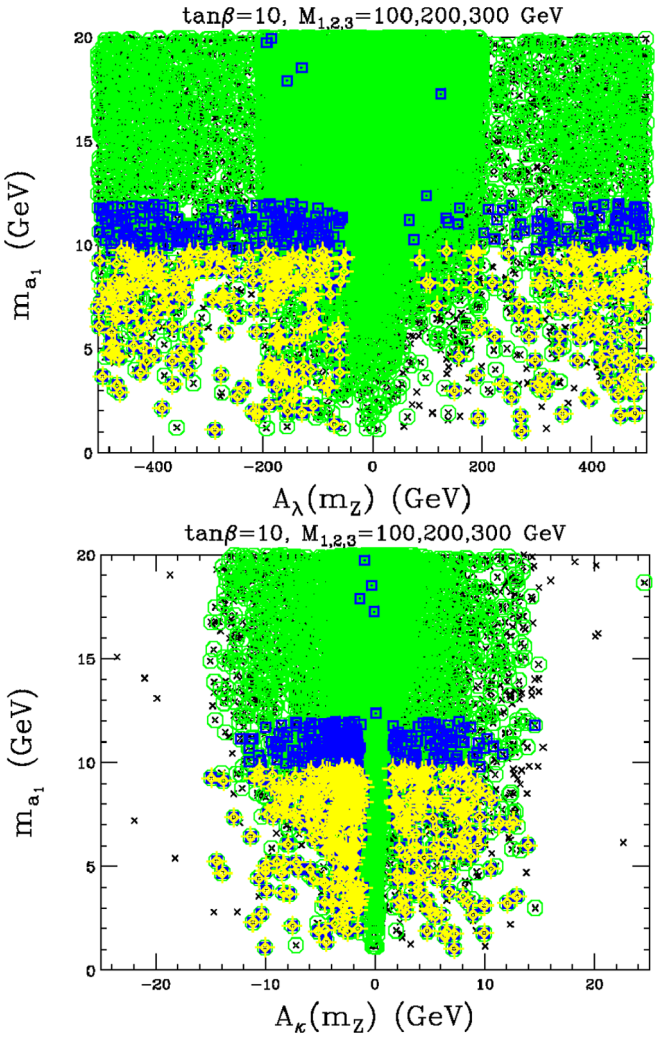

FIG. 22 (color online). m_{a_1} vs $A_\lambda(m_Z)$ and $A_\kappa(m_Z)$ for points with $F < 50$ taking $M_{1,2,3}(m_Z) = 100, 200, 300$ GeV and $\tan\beta = 10$. Point notation as in Fig. 6.

following plots that the reader can match points from one plot to another.

First, we show F as a function of m_{h_1} and m_{a_1} in Fig. 28. In the upper plot, we see again the preference for m_{h_1} near 100 GeV. The lower plot shows that the very smallest F values occur at m_{a_1} values above $2m_\tau$, implying that the $a_1 \to \tau^+\tau^-$ channel is the dominant a_1 decay. We note that the $2m_\tau < m_{a_1}$ part of the $m_{a_1} < 2m_b$ fully okay zone was also found in the companion paper [10] to be preferred in order to avoid fine-tuning associated with getting small m_{a_1}.

One important prediction of any given parameter set is that for $\xi^2(Z + b's)$, where

$$\xi^2(Z + b's) \equiv \frac{g^2_{ZZh_1}}{g^2_{ZZh_{\rm SM}}}[B(h_1 \to b\bar{b}) + B(h_1 \to a_1a_1) \times [B(a_1 \to b\bar{b})]^2]. \quad (26)$$

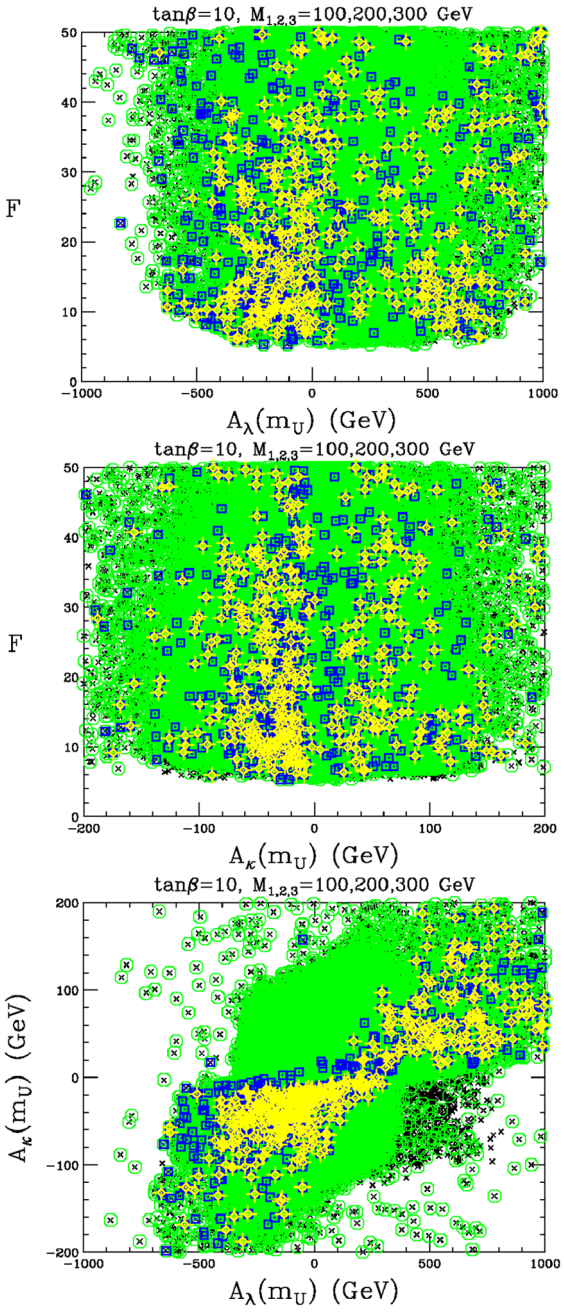

FIG. 23 (color online). F vs $A_\lambda(M_U)$ and $A_\kappa(M_U)$ (upper two plots) and $A_\kappa(M_U)$ vs $A_\lambda(M_U)$ (lower plot) for points with $F < 50$ taking $M_{1,2,3}(m_Z) = 100, 200, 300$ GeV and $\tan\beta = 10$. Point notation as in Fig. 6.

For the fully okay points one has $m_{a_1} < 2m_b$ and thus $\xi^2(Z + b's) = C^{2b}_{\rm eff}$. More generally, $\xi^2(Z + b's)$ is the net rate for LEP production of $Z + 2b$ *and* $Z + 4b$ final states relative to the rate that one would obtain for a SM Higgs boson which decayed entirely to $b\bar{b}$. Of particular interest is the correlation between $\xi^2(Z + b's)$ and F. Thus, an important comparison is the model prediction for $\xi^2(Z + b's)$ relative to the excess found at LEP in the vicinity of $b\bar{b}$ mass $\sim$100 GeV. The value of

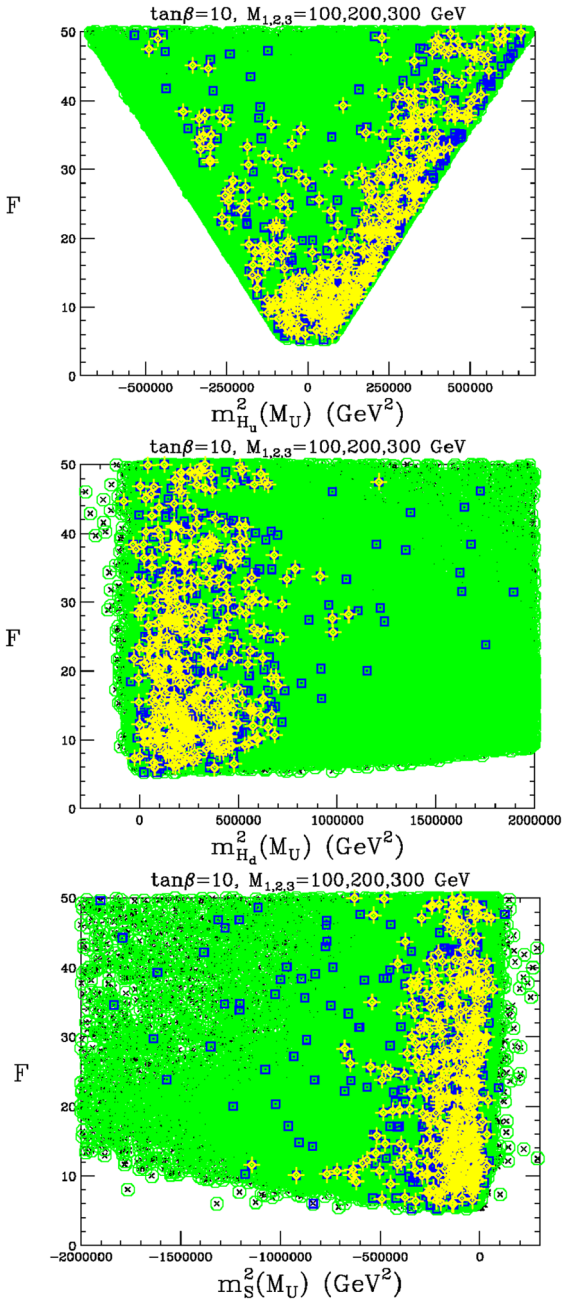

FIG. 24 (color online). Fine-tuning vs $m^2_{H_u}(M_U)$, $m^2_{H_d}(M_U)$, and $m^2_S(M_U)$ for points with $F < 50$ taking $M_{1,2,3}(m_Z) = 100$, 200, 300 GeV and $\tan\beta = 10$. Point notation as in Fig. 6.

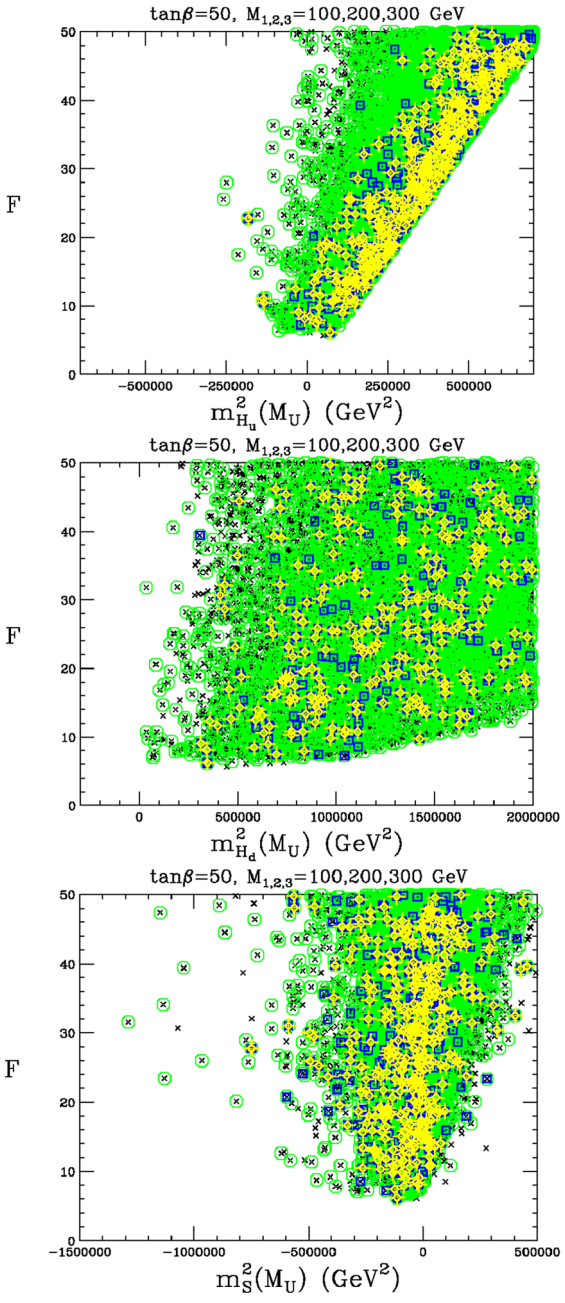

FIG. 25 (color online). Fine-tuning vs $m^2_{H_u}(M_U)$, $m^2_{H_d}(M_U)$, and $m^2_S(M_U)$ for points with $F < 50$ taking $M_{1,2,3}(m_Z) = 100$, 200, 300 GeV and $\tan\beta = 50$. Point notation as in Fig. 6.

$\xi^2(Z + b's) = C^{2b}_{\rm eff}$ as a function of m_{h_1} is plotted in Fig. 29. We observe that the points with $F < 10$ lie in the range $C^{2b}_{\rm eff} \lesssim 0.2$ with many of the very lowest F points having $C^{2b}_{\rm eff} \in [0.07, 0.13]$, the range most consistent with the LEP excess at bb mass $\sim$98 GeV.

Next, we wish to illustrate the relative MSSM vs singlet composition of the a_1 and h_1 for the $F < 10$ points. This composition has obvious implications for their couplings to SM particles. The more pure MSSM the h_1 is, the more SM-like will be its couplings. The more singlet the a_1 is, the more weakly it will be coupled to SM particles. In particular, its couplings to SM down-type fermions and leptons are given by $\tan\beta\cos\theta_A$ times the SM-like weight in which $\bar{b}1b$ is replaced by $\bar{b}i\gamma_5 b$, for example. These compositions are shown in Fig. 30. The upper plot illustrates that there is a lower bound on $|\cos\theta_A|$ that arises from the joint requirements of large $B(h_1 \to a_1 a_1)$ and $m_{a_1} < 2m_b$. As noted earlier, this guarantees that the $b\bar{b}$ (and $\tau^+\tau^-$) coupling strengths of the a_1 are sufficiently large that the decays of the a_1 are dominated by the

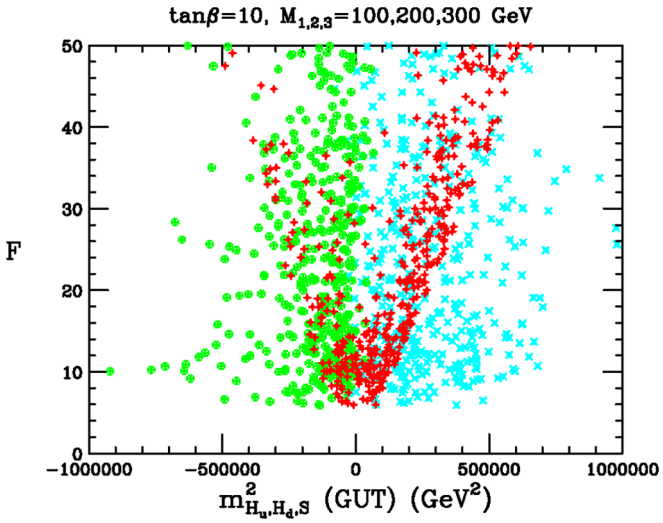

FIG. 26 (color online). Fine-tuning vs the GUT-scale soft Higgs masses squared for points with $F < 50$ taking $M_{1,2,3}(m_Z) = 100$, 200, 300 GeV and $\tan\beta = 10$. Point notation: dark (red) $m^2_{H_u}(M_U)$; light gray (cyan) $m^2_{H_d}(M_U)$; darker gray (green) $m^2_S(M_U)$. Points plotted are the yellow fancy cross points from Fig. 24.

heaviest fermionic states, i.e. $a_1 \to \tau^+\tau^-$ for $2m_\tau < m_{a_1} < 2m_b$ and $a_1 \to c\bar{c}$ for $2m_c < m_{a_1} < 2m_\tau$, with $a_1 \to gg$ also being important. For $m_{a_1} < 2m_c$, $a_1 \to gg$ is the dominant decay. Note the preference for $\cos\theta_A \sim -0.1$ for the very lowest F points. The lower plot of Fig. 30 shows the singlet component, $\sin\theta_S$, of the h_1 for the fully okay solutions. The h_1 can be as much as 20% singlet at the amplitude level, but this means it is still 96% nonsinglet in the amplitude-squared sense. As a result, all plotted points have $|C_V| \sim 1$. The very lowest F points are clearly associated with very small $\sin\theta_S$.

We now turn to the GUT-scale parameters associated with $F < 10$ large yellow fancy cross points (plotted as blue +'s for these figures) that pass all experimental constraints and the correlations among them.

First, we consider $\kappa(M_U)$ and $\lambda(M_U)$ in Fig. 31. We see that the very lowest F values have fairly small $\lambda(M_U)$ and significantly larger $\kappa(M_U) \sim -0.4$.

We consider $A_\kappa(M_U)$ and $A_\lambda(M_U)$ in Fig. 32. We see that the very lowest F values have fairly small $A_\lambda(M_U)$ and $A_\kappa(M_U)$, i.e., as noted earlier, both are close to being consistent with no-scale boundary conditions at M_U.

We consider $m_{H_u}(M_U)$, $m_{H_d}(M_U)$, and $m_S(M_U)$ in Fig. 33. We see that the very lowest F values have fairly small GUT-scale values for all the scalar Higgs mass

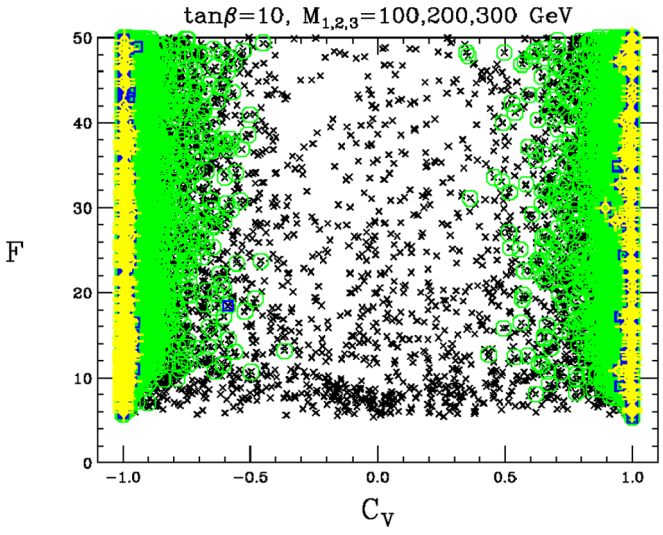

FIG. 27 (color online). Fine-tuning vs the relative coupling strength, $C_V \equiv g_{h_1WW}/g_{h_{SM}WW}$ for $\tan\beta = 10$. Point notation as in Fig. 6.

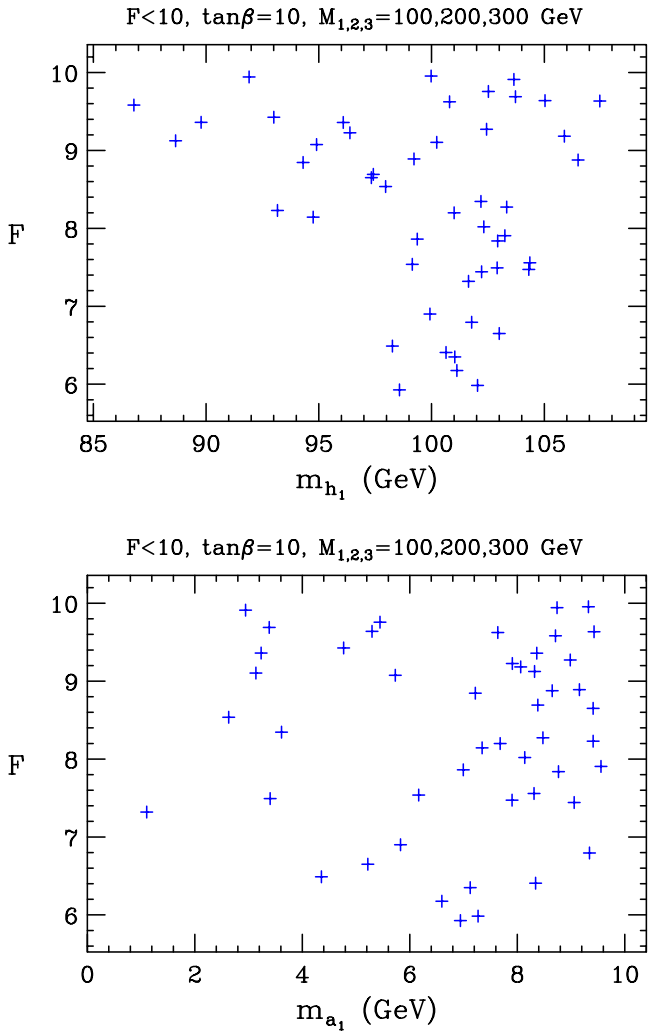

FIG. 28 (color online). The upper plot shows fine-tuning vs m_{h_1} for the large (yellow) cross points (for clarity, we use blue +'s in their place in this and succeeding plots) with $F < 10$ taking $M_{1,2,3}(m_Z) = 100$, 200, 300 GeV and $\tan\beta = 10$. The lower plot shows F vs m_{a_1}.

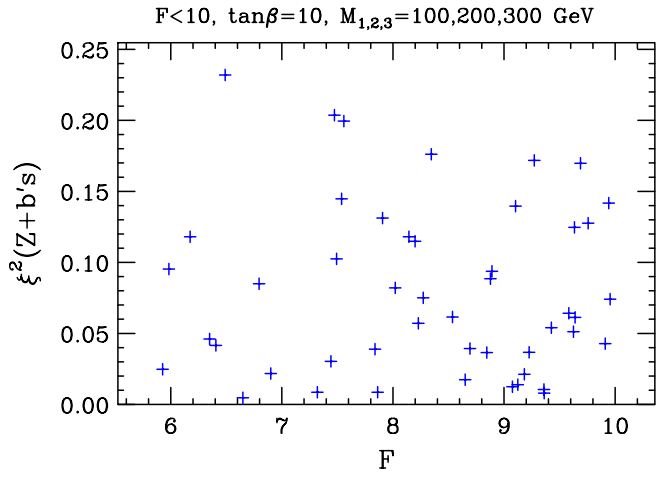

FIG. 29 (color online). The plot shows $\xi^2(Z + b's)$ (which equals $C_{\rm eff}^{2b}$ since $C_{\rm eff}^{4b} = 0$ when $m_{a_1} < 2m_b$) vs F for the large (yellow) cross points with $F < 10$ taking $M_{1,2,3}(m_Z) = 100, 200, 300$ GeV and $\tan\beta = 10$.

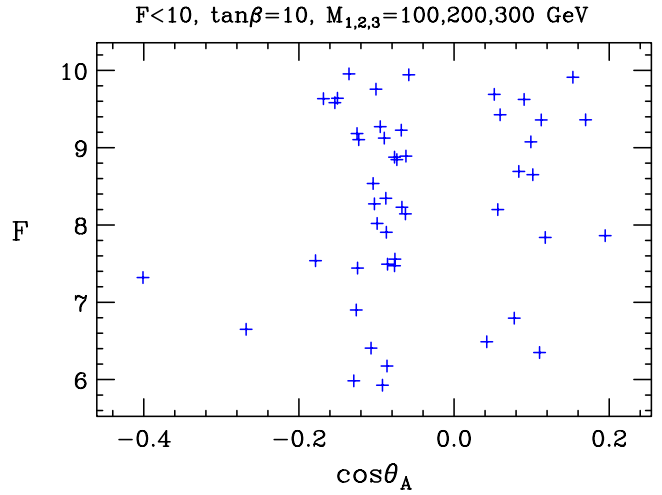

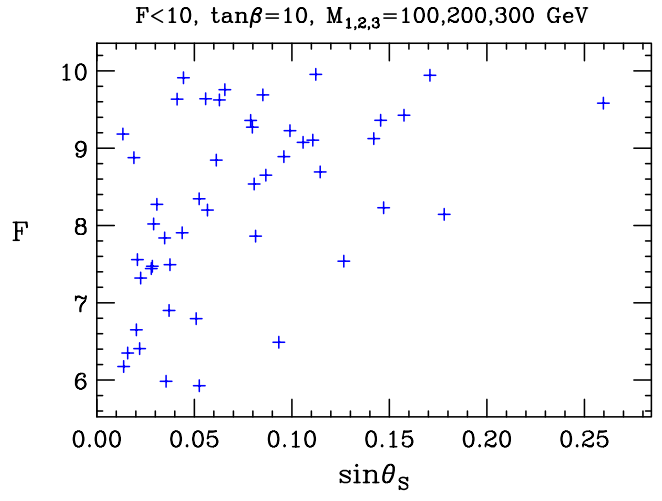

FIG. 30 (color online). The plots show F vs $\cos\theta_A$ (upper) and F vs $\sin\theta_S$ (lower) for the large (yellow) cross points with $F < 10$ taking $M_{1,2,3}(m_Z) = 100, 200, 300$ GeV and $\tan\beta = 10$.

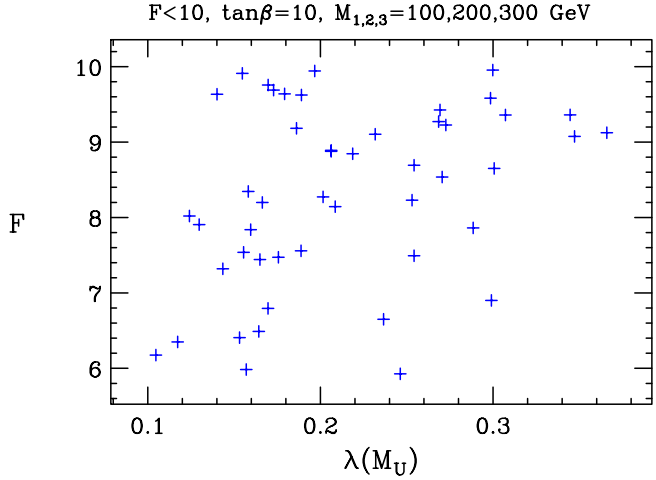

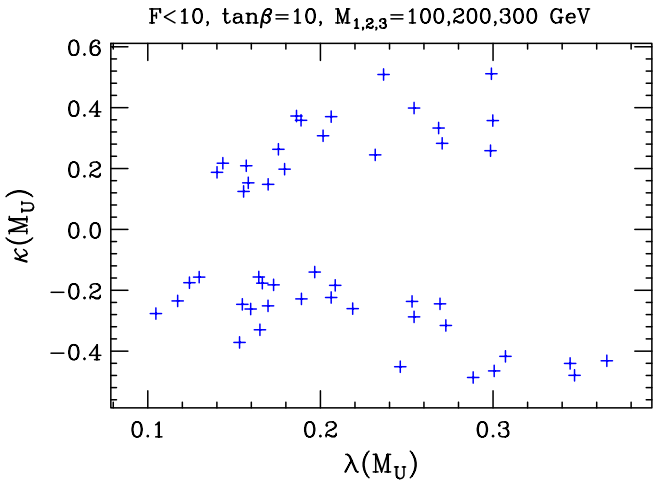

FIG. 31 (color online). The upper plot shows fine-tuning vs $\lambda(M_U)$ for large (yellow) cross points with $F < 10$ taking $M_{1,2,3}(m_Z) = 100$, 200, 300 GeV and $\tan\beta = 10$. The lower plot shows $\kappa(M_U)$ as a function of $\lambda(M_U)$.

squared values, again close to being consistent with no-scale boundary conditions at M_U. However, our scans did not locate any fully okay points for which $m_{H_u}(M_U)$, $m_{H_d}(M_U)$, and $m_S(M_U)$ were all simultaneously small. We are unsure at this time as to whether this is an artifact of limited computer time for scanning or something deeper.

IV. MODERATELY LOW F POINTS WITH DOMINANT $a_1 \to \gamma\gamma$ DECAYS

Let us now turn to the special class of points mentioned in Sec. II. These are the low-F points with a SM-like h_1 of mass $\sim$100 GeV and for which $m_{a_1} \gtrsim 30$ GeV. For these points, $B(h_1 \to a_1 a_1) > 0.75$ and $B(a_1 \to \gamma\gamma) \gtrsim 0.9$. For this to occur, the a_1 must be highly singlet in nature so that the tree-level decays to fermion-antifermion are highly suppressed, in which case the chargino loop-induced decay to $\gamma\gamma$ can be dominant. (The relevant couplings are present even when the a_1 is purely singlet.) This combination of

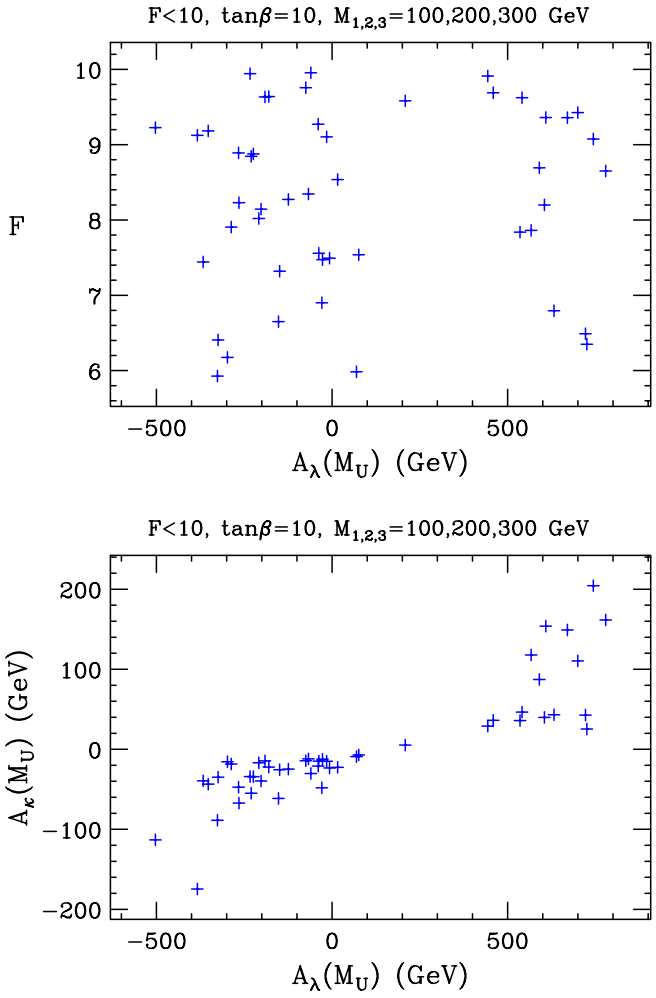

FIG. 32 (color online). The upper plot shows fine-tuning vs $A_\lambda(M_U)$ for fully okay points with $F < 10$ taking $M_{1,2,3}(m_Z) =$ 100, 200, 300 GeV and $\tan\beta = 10$. The lower plot shows $A_\kappa(M_U)$ as a function of $A_\lambda(M_U)$.

features allows consistency with the LEP limits on the $Z + b's$ channel. We have not been able to determine if there are relevant limits on the $Z + 4\gamma$ channel. This channel would have quite a high rate and most probably these relatively spectacular events would have been noticed. These points are also disfavored theoretically since, as detailed shortly, a very high level of fine-tuning of GUT-scale parameters is required in order to achieve $\cos\theta_A \lesssim 10^{-4}$ as required (for $\tan\beta = 10$) for $a_1 \to 2\gamma$ to be the dominant a_1 decay channel. Nonetheless, they should not be entirely discarded as a possible class and so we give some details regarding them in the following. These points were found using an extremely fine grid scanning approach of the type detailed in [10] with fixed $m_{\rm SUSY} = -A_t =$ 300 GeV, $\mu = 150$ GeV, and $\tan\beta = 10$.

Basic plots for this scenario appear in Fig. 34. The top plot of this figure gives F as a function of m_{h_1}. We see again that $m_{h_1} \sim 100$ GeV gives the lowest F value, $F \sim 11$ in this case. The lower plot shows that $m_{a_1} \gtrsim 30$ TeV is

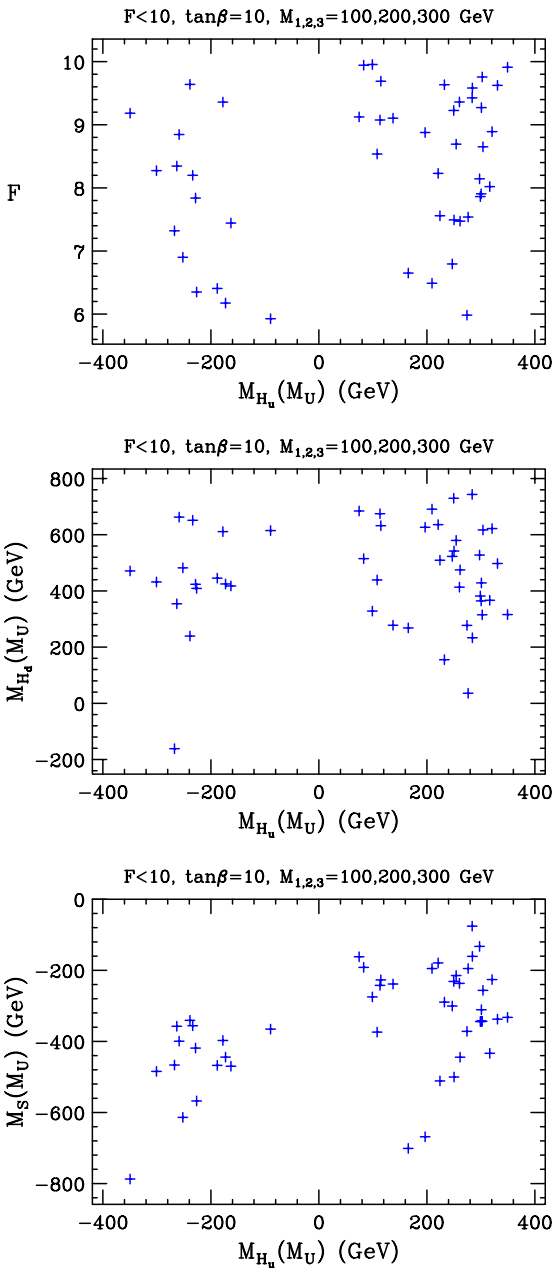

FIG. 33 (color online). The upper plot shows fine-tuning vs $m_{H_u}(M_U)$ for fully okay points with $F < 10$ taking $M_{1,2,3}(m_Z) =$ 100, 200, 300 GeV and $\tan\beta = 10$. The middle plot shows $m_{H_d}(M_U)$ as a function of $m_{H_u}(M_U)$. The bottom plot shows $m_S(M_U)$ as a function of $m_{H_u}(M_U)$. Our convention is that if an M^2 is negative then we plot $-\sqrt{-M^2}$.

required for this kind of scenario, with the lowest F obtained for $m_{a_1} \sim 30$ GeV. Figure 35 shows F vs $\cos\theta_A$ as the top plot, $B(a_1 \to \gamma\gamma)$ as a function of $\cos\theta_A$ as the middle plot and $\xi^2(Z + b's)$ vs m_{h_1} as the bottom plot. The top plot is useful for correlating F with the value of $\cos\theta_A$. However, note that there is some degeneracy: essentially the same values of F and $\cos\theta_A$ are sometimes obtained even though the basic scan parameters are different. The

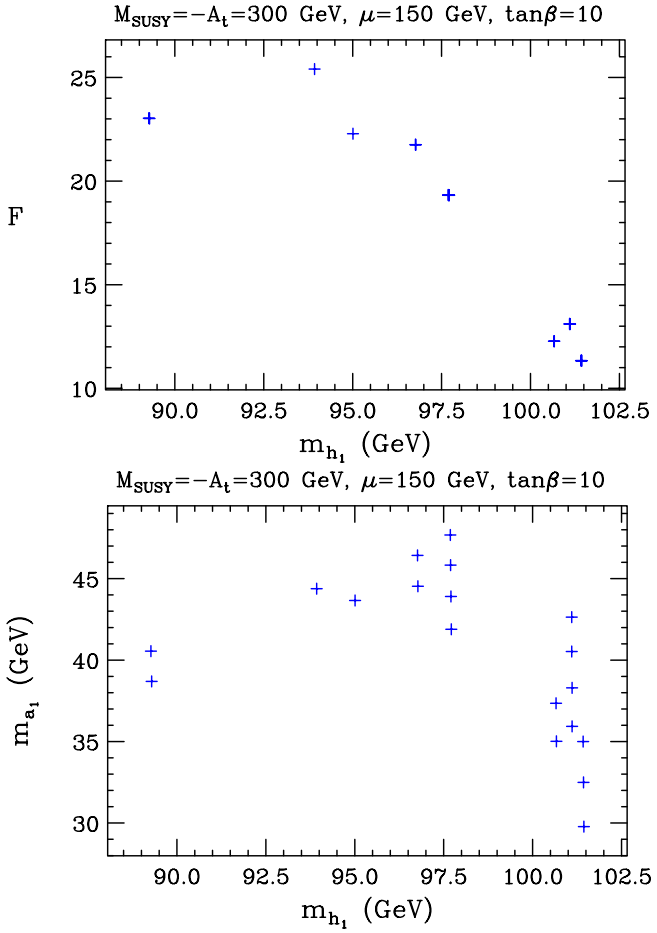

FIG. 34 (color online). For the points with dominant $a_1 \to \gamma\gamma$ decays and low F, we plot: F vs m_{h_1} (top); and m_{a_1} vs m_{h_1} (bottom). Note that there are a number of degeneracies where exactly the same F and m_{h_1} are predicted for somewhat different parameter choices in the scan.

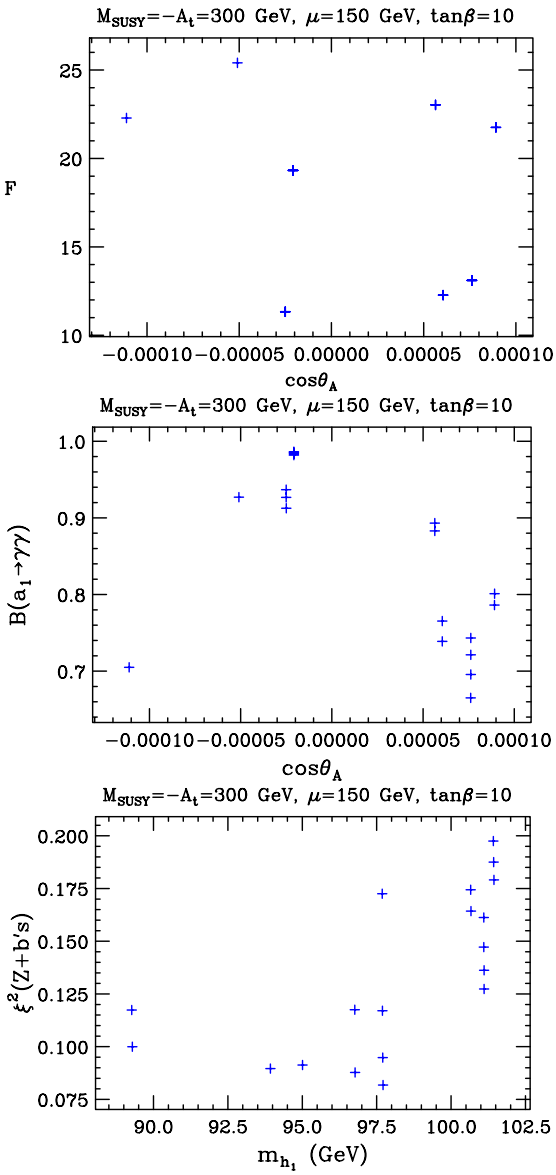

FIG. 35 (color online). For the points with dominant $a_1 \to \gamma\gamma$ decays and low F, we plot: F vs $\cos\theta_A$ (top); $B(a_1 \to \gamma\gamma)$ vs $\cos\theta_A$ (middle); and $\xi^2(Z + b's)$ vs m_{h_1} (bottom). Since F depends primarily on $\cos\theta_A$, there are a number of points in the F vs $\cos\theta_A$ plot that are actually multiple repetitions of exactly the same F at a given $\cos\theta_A$ value but with $B(a_1 \to \gamma\gamma)$ and $\xi^2(Z + b's)$ varying slightly because of sensitivity to other parameters of the scan.

middle plot shows that $B(a_1 \to \gamma\gamma) \gtrsim 0.65$ for these points, with $B(a_1 \to \gamma\gamma) \sim 0.65$ for the $F \sim 11$ points. As expected, very small $\cos\theta_A$ is required in order for the $a_1 \to \gamma\gamma$ decays to be dominant. The bottom plot of the figure shows $\xi^2(Z + b's)$ as a function of m_{h_1}. We observe that $\xi^2(Z + b's)$ is of the right general magnitude to explain the LEP excess for the lowest F points that have $m_{h_1} \sim 101$ GeV. We note that $\xi^2(Z + b's)$ receives contributions from both the $Z + 2b$ final state from direct $h_1 \to b\bar{b}$ decay and also the $Z + 4b$ from $h_1 \to a_1 a_1 \to 4b$ where $B(a_1 \to b\bar{b}) < 0.35$ due to the competition from the $a_1 \to \gamma\gamma$ decays.

The careful reader may wonder why it is that we can have small $\cos\theta_A$ for these points whereas the $m_{a_1} < 2m_b$ points have a lower bound on $\cos\theta_A$. In fact, it is precisely the *combination* of the requirements that $m_{a_1} < 2m_b$ and $B(h_1 \to a_1 a_1) \gtrsim 0.75$ which forces a lower bound on $\cos\theta_A$. Values of $\cos\theta_A$ small enough to yield large $B(a_1 \to \gamma\gamma)$ while at the same time $B(h_1 \to a_1 a_1) \gtrsim 0.7$ is maintained are only possible for relatively large m_{a_1}.

The fine-tuning required in A_λ and A_κ to achieve very small $\cos\theta_A$ can be quantified via the derivatives

$$F_{A_\lambda}^{\cos\theta_A} \equiv \frac{\partial \cos\theta_A}{\partial A_\lambda} \frac{A_\lambda}{\cos\theta_A}, \qquad F_{A_\kappa}^{\cos\theta_A} \equiv \frac{\partial \cos\theta_A}{\partial A_\kappa} \frac{A_\kappa}{\cos\theta_A}, \tag{27}$$

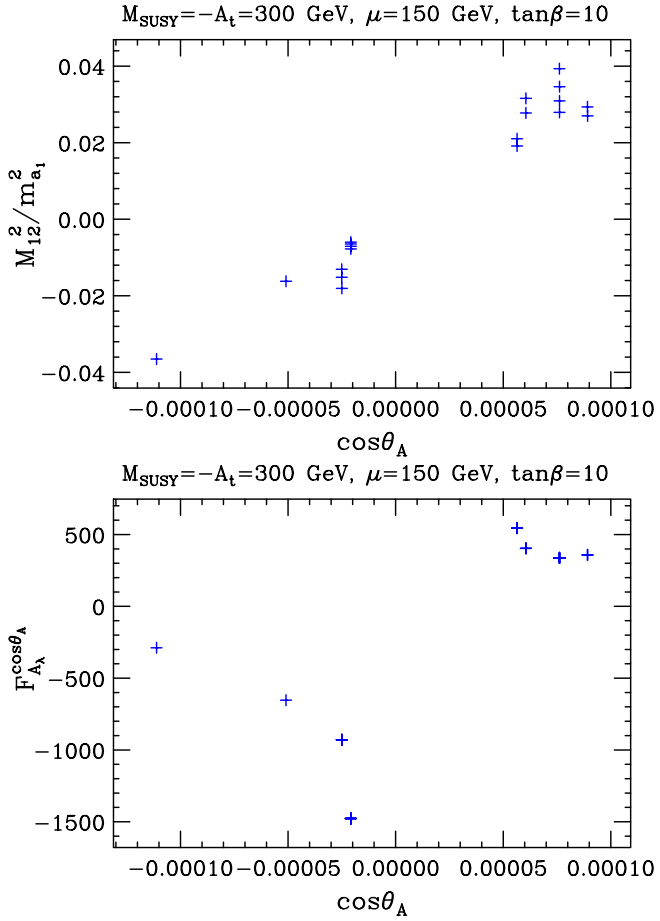

FIG. 36 (color online). For the points with dominant $a_1 \to \gamma\gamma$ decays and low F, we plot: $M_{12}^2/m_{a_1}^2$ vs $\cos\theta_A$ (top); and $F_{A_\lambda}^{\cos\theta_A}$ as a function of $\cos\theta_A$ (bottom). (Many of the points have the same $F_{A_\lambda}^{\cos\theta_A}$ value.)

where all parameters are defined at scale m_Z. Understanding of these quantities can be gleaned from the approximate formula

$$\cos\theta_A \simeq -\frac{M_{12}^2}{M_{11}^2 - M_{22}^2} \simeq -\frac{\lambda v(A_\lambda - 2\kappa s)\sin 2\beta}{2\lambda s(A_\lambda + \kappa s) + 3\kappa A_\kappa s \sin 2\beta}, \quad (28)$$

where we used[3]

$$M_{11}^2 = \frac{2\lambda s}{\sin 2\beta}(A_\lambda + \kappa s), \quad (29)$$

$$M_{12}^2 = \lambda v(A_\lambda - 2\kappa s), \quad (30)$$

$$M_{22}^2 = 2\lambda\kappa v^2 \sin 2\beta + \lambda A_\lambda \frac{v^2 \sin 2\beta}{2s} - 3\kappa A_\kappa s. \quad (31)$$

Equation (28) shows that there will be great sensitivity of $\cos\theta_A$ to the value of A_λ relative to $2\kappa s$, and almost no sensitivity to A_κ. Both are confirmed by the numerical results we now present for fixed $M_{1,2,3} = 100$, 200, 300 GeV, $\tan\beta = 10$, $\mu_{\rm eff} = 150$ GeV, $A_t = -300$ GeV, $A_b = A_\tau = 0$, $M_{Q,U,D,L,E} = 300$ GeV (for the relevant 3rd generation). Different points are obtained by scanning in λ, κ, A_λ, A_κ. (Obviously, many more 4γ points could be found if the fixed parameters are allowed to vary. However, large $A_t < 0$ is essential to get small F for such points.)

In Fig. 36, we plot $M_{12}^2/m_{a_1}^2$ vs $\cos\theta_A$ and $F_{A_\lambda}^{\cos\theta_A}$ vs $\cos\theta_A$. The top plot shows that $M_{12}^2/m_{a_1}^2$ must be small for small $\cos\theta_A$ (and there is a strong linear relation). The bottom plot shows that such small values of $\cos\theta_A$ imply rather large values of $F_{A_\lambda}^{\cos\theta_A}$. Given Eq. (23), high sensitivity to the m_Z-scale value of A_λ implies a high level of fine-tuning for A_λ (at scale m_Z) with respect to $A_\lambda(M_U)$,

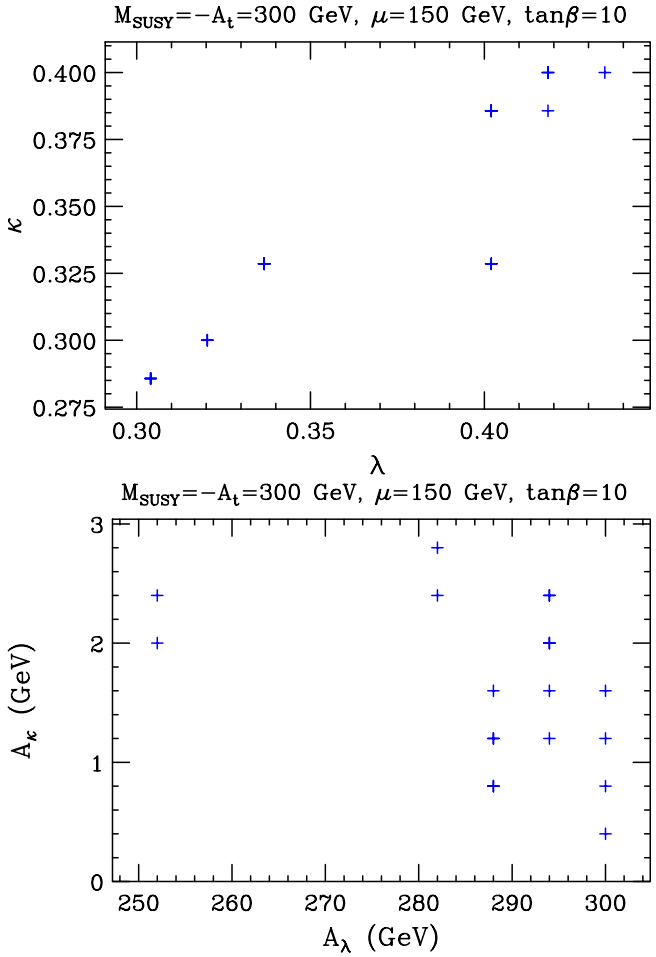

FIG. 37 (color online). For the points with dominant $a_1 \to \gamma\gamma$ decays and low F, we plot: κ vs λ (top); and A_κ vs A_λ (bottom).

[3]These mass squared matrix entries receive radiative corrections not shown here.

$A_t(M_U)$ and $M_3(M_U)$. One should also note that the $F_{A_\lambda}^{\cos\theta_A}$ tuning measure for A_λ is largest (~ -1500) for the point for which the electroweak symmetry breaking fine-tuning measure F is smallest and vice-versa.

Finally, the two plots of Fig. 37 show that these points require largish κ and λ that are fairly closely correlated, while A_κ must be quite small.

V. CONCLUSIONS

There is strong motivation for a supersymmetric model with an extended Higgs sector containing one or more extra Higgs singlet superfields. These motivations range from string theory model building, where it is known that SM-singlets are abundant in string theory compactifications, to the purely phenomenological, including the fact that adding anything other than SM singlets to the MSSM will typically destroy gauge coupling unification. In this paper, we have studied in detail the next-to-minimal supersymmetric model, which contains exactly one singlet Higgs superfield in addition to the two Higgs doublet superfields of the MSSM. We have shown that there is a portion of NMSSM parameter space with an abundance of attractive features, no outstanding problems and which leads to an important set of predictions that should be taken quite seriously. There are many ways in which the NMSSM is a better benchmark theory than the MSSM, since it has important flexibilities that are currently leading to problematical issues for the MSSM. The attractive features of the NMSSM include:

(i) a natural explanation for the μ parameter is provided—since all superpotential couplings are dimensionless in the NMSSM, the scale of μ is given by the scale of soft-SUSY-breaking, which (see below) can be well below a TeV;

(ii) the supersymmetric context provides a highly satisfactory solution of the naturalness/hierarchy problem if the squark masses (in particular, the stop masses) and the gluino mass are well below a TeV (implying possible discovery at the Tevatron and very plentiful production at the LHC);

(iii) in particular, such squark masses imply that fine-tuning with respect to GUT-scale parameters is not required in order to obtain the observed value of m_Z and a light SM-like Higgs boson;

(iv) low squark masses imply that the lightest Higgs boson, the h_1, will most naturally be SM-like in its couplings to SM particles and have a mass of order 100 GeV, close to the ideal value for satisfying precision electroweak constraints;

(v) LEP data is fully consistent with such an h_1 provided it decays mostly via $h_1 \to a_1 a_1 \to \tau^+\tau^-\tau^+\tau^-$ (requiring $2m_\tau < m_{a_1} < 2m_b$) or $h_1 \to a_1 a_1 \to 4j$ (when $m_{a_1} < 2m_\tau$), where the a_1 is primarily the CP-odd component of the extra complex scalar Higgs singlet field;

(vi) an appropriately large value of $B(h_1 \to a_1 a_1)$ is typically such that $B(h_1 \to b\bar{b}) \sim 0.1$, thereby providing a natural explanation for the event excess near 98 GeV in LEP data for the $Z + b\bar{b}$ channel;

(vii) it is quite natural for the a_1 to be lighter than $2m_b$ while at the same time having sufficient $h_1 a_1 a_1$ coupling for large $B(h_1 \to a_1 a_1)$;

(viii) the optimal scenarios fit nicely with choices for the GUT-scale values of the soft-SUSY-breaking Higgs masses squared and A parameters that are quite modest in size, as might be associated with an approximate no-scale model for SUSY breaking;

(ix) in the natural scenarios above, the heavier Higgs bosons of the model (two CP-even and one CP-odd neutral Higgs bosons and the charged Higgs boson) have relatively modest masses that would make them accessible at a hadron collider if $\tan\beta$ is large enough and mostly accessible at a 1 TeV linear e^+e^- collider;

(x) the light mostly-singlet a_1 must have a minimum coupling to the SM particles (through mixing with the nonsinglet CP-odd state) that implies a lower bound, albeit small, on $B(\Upsilon \to \gamma a_1)$;

(xi) the a_1 could allow for adequate annihilation in the early universe of very light neutralinos [23].

The attractiveness of this scenario suggests that the LEP groups should push a reanalysis of the $Z4\tau$ channel in the hope of either ruling out the $h_1 \to a_1 a_1 \to 4\tau$ scenario, or finding an excess consistent with it for m_{h_1} in the vicinity of 100 GeV. Either a positive or negative result would have very important implications for Higgs searches at the Tevatron and LHC. We also stress that B factory experiments should attempt to search for a $\Upsilon \to \gamma a_1$ signal down to the lowest possible branching ratio (the predicted minimum in the NMSSM context being of order 10^{-7}).

We speculate that similar results could emerge in other supersymmetric models with a Higgs sector that, like the case of the NMSSM, is more complicated than that of the MSSM. Many such models can be constructed. Thus, much of the discussion above regarding Higgs discovery is quite generic. In general, there might be quite a few light a's, all of which could appear in the decay of a light SM-like h and all of which would provide potential signals in reanalyzed LEP data and in $\Upsilon \to \gamma a$ decays. There is a potential goldmine of discovery if one digs deeply enough.

However, whether the a is truly the NMSSM CP-odd a_1 or just a lighter Higgs boson into which the SM-like h pair-decays, hadron collider detection of the h in its $h \to aa$ decay mode will be very challenging. Discovery modes that one can hope to demonstrate to be viable include:

(i) WW fusion—$WW \to h \to aa \to 4\tau$;

(ii) $t\bar{t}h$ production with $h \to aa \to 4\tau$;

(iii) diffractive production [24], $pp \to pph$, with $h \to aa \to 4\tau$. This latter mode looks very promising [25].

Unfortunately, it seems very doubtful that viable discovery signals would be possible for the analogous modes with $h \to aa \to 4$ jet (that would be the only ones available if $m_a < 2m_\tau$). Although $m_a > 2m_\tau$ is somewhat preferred by naturalness arguments in the NMSSM case, one should be prepared for the possibility that the LHC will discover a plethora of supersymmetric particles, and perhaps some heavy Higgs bosons (if $\tan\beta$ is large enough) but fail to see the SM-like light Higgs most closely associated with electroweak symmetry breaking. The only LHC evidence for its existence would then be that WW scattering would be found to be fully perturbative, as predicted if there is a light h with SM-like couplings to WW.

At a linear collider, detection of $e^+e^- \to Zh$ production using the $e^+e^- \to ZX$ missing mass M_X approach will be completely straightforward. A 100 GeV h with SM coupling to ZZ will result in many events forming a sharp peak in M_X, quite independently of how the h decays. The decays can then be analyzed to see what is present and with what branching ratio. Detection of an h with unexpected decays at a photon collider will also be reasonably straightforward [26].

ACKNOWLEDGMENTS

This work was supported by the U.S. Department of Energy under grants DE-FG02-90ER40542 and DE-FG03-91ER40674. JFG thanks the Aspen Center for Physics where part of this work was performed.

[1] R. Barate *et al.* (LEP Working Group for Higgs boson searches), Phys. Lett. B **565**, 61 (2003).
[2] R. Dermisek and J. F. Gunion, Phys. Rev. Lett. **95**, 041801 (2005).
[3] R. Dermisek and J. F. Gunion, Phys. Rev. D **73**, 111701 (2006).
[4] We thank P. Bechtle for processing our low-F points through the full preliminary LHWG analysis package.
[5] J. F. Gunion, H. E. Haber, and T. Moroi, arXiv:hep-ph/9610337.
[6] B. A. Dobrescu, G. Landsberg, and K. T. Matchev, Phys. Rev. D **63**, 075003 (2001); B. A. Dobrescu and K. T. Matchev, J. High Energy Phys. 09 (2000) 031.
[7] U. Ellwanger, J. F. Gunion, and C. Hugonie, arXiv:hep-ph/0111179; U. Ellwanger, J. F. Gunion, C. Hugonie, and S. Moretti, arXiv:hep-ph/0305109; arXiv:hep-ph/0401228.
[8] D. J. Miller and S. Moretti, arXiv:hep-ph/0403137.
[9] U. Ellwanger, J. F. Gunion, and C. Hugonie, J. High Energy Phys. 07 (2005) 041.
[10] R. Dermisek and J. F. Gunion, Phys. Rev. D **75**, 075019 (2007).
[11] LEP Working Group for Higgs Boson Searches, LHWG Report No. LHWG-Note 2005-01.
[12] M. Carena, J. R. Ellis, A. Pilaftsis, and C. E. M. Wagner, Phys. Lett. B **495**, 155 (2000); A. Sopczak, Int. J. Mod. Phys. A **16S1B**, 816 (2001); Yad. Fiz. **65**, 2179 (2002) [Phys. At. Nucl. **65**, 2116 (2002)]; Nucl. Phys. B, Proc. Suppl. **109**, 271 (2002); G. L. Kane, T. T. Wang, B. D. Nelson, and L. T. Wang, Phys. Rev. D **71**, 035006 (2005); M. Drees, Phys. Rev. D **71**, 115006 (2005); S. G. Kim, N. Maekawa, A. Matsuzaki, K. Sakurai, A. I. Sanda, and T. Yoshikawa, Phys. Rev. D **74**, 115016 (2006); A. Belyaev, Q. H. Cao, D. Nomura, K. Tobe, and C. P. Yuan, arXiv:hep-ph/0609079.
[13] H. P. Nilles, M. Srednicki, and D. Wyler, Phys. Lett. **120B**, 346 (1983); J. M. Frere, D. R. T. Jones, and S. Raby, Nucl. Phys. **B222**, 11 (1983); J. P. Derendinger and C. A. Savoy, Nucl. Phys. **B237**, 307 (1984); J. R. Ellis, J. F. Gunion, H. E. Haber, L. Roszkowski, and F. Zwirner, Phys. Rev. D **39**, 844 (1989); M. Drees, Int. J. Mod. Phys. A **4**, 3635 (1989); U. Ellwanger, M. Rausch de Traubenberg, and C. A. Savoy, Phys. Lett. B **315**, 331 (1993); Nucl. Phys. **B492**, 21 (1997); S. F. King and P. L. White, Phys. Rev. D **52**, 4183 (1995); F. Franke and H. Fraas, Int. J. Mod. Phys. A **12**, 479 (1997).
[14] U. Ellwanger, J. F. Gunion, and C. Hugonie, J. High Energy Phys. 02 (2005) 066.
[15] M. Bastero-Gil, G. L. Kane, and S. F. King, Phys. Lett. B **474**, 103 (2000).
[16] G. L. Kane and S. F. King, Phys. Lett. B **451**, 113 (1999).
[17] R. Dermisek and H. D. Kim, Phys. Rev. Lett. **96**, 211803 (2006).
[18] R. Dermisek and J. F. Gunion, arXiv:0709.2269.
[19] M. Bastero-Gil, C. Hugonie, S. F. King, D. P. Roy, and S. Vempati, Phys. Lett. B **489**, 359 (2000).
[20] G. Hiller, Phys. Rev. D **70**, 034018 (2004).
[21] R. Dermisek, J. F. Gunion, and B. McElrath, Phys. Rev. D **76**, 051105 (2007).
[22] Some recent estimates for CMS are found in S. Gennai, S. Heinemeyer, A. Kalinowski, R. Kinnunen, S. Lehti, A. Nikitenko, and G. Weiglein, arXiv:hep-ph/0704.0619. A summary of Tevatron limits is given in A. Anastassov (CDF and D0 Collaborations), Proc. Sci., HEP2005 (2006) 326.
[23] J. F. Gunion, D. Hooper, and B. McElrath, Phys. Rev. D **73**, 015011 (2006).
[24] A. D. Martin, V. A. Khoze, and M. G. Ryskin, arXiv:hep-ph/0507305; J. R. Forshaw, arXiv:hep-ph/0508274; A. B. Kaidalov, V. A. Khoze, A. D. Martin, and M. G. Ryskin, Eur. Phys. J. C **33**, 261 (2004).
[25] J. F. Gunion, V. Khoze, A. deRoeck, and M. Ryskin (unpublished).
[26] J. F. Gunion and M. Szleper, arXiv:hep-ph/0409208.